



*Comparative Study of the Electrochemical and the Optical Band Gap  
of Organic Semiconductors*

Diplomarbeit zur Erlangung des akademischen Grades

*Diplomingenieur*

in der Studienrichtung *Wirtschaftsing.wesen Technische Chemie*

Angefertigt am *Linzer Institut für Organische Solarzellen (LIOS)*

Betreuung:

*Prof. Dr. Serdar Niyazi Sariciftci*

Von:

*David Mühlbacher*

Mitbetreuung:

*Dr. Helmut Neugebauer*

*Linz, September 2002*

I want to thank all the people who supported and helped me to prepare this work:

- All the members of the “Linzer Institute for Organic Solar Cells” LIOS, Andrej Andreev, Elif Arici, Eugen Baumgartner, Antonio Cravino, Harald Hoppe, Markus Koppe, Maria Antonietta Loi, Gebhard Matt, Dieter Meissner, Markus Scharber and Christoph Winder all of them for fruitful discussions and suggestions and especially Antonio Cravino and Markus Scharber for experimental help
- The staff of QSEL Patrick Denk, Attila Mozer, Franz Padinger, Roman Rittberger and Elisabeth Wirtl for the friendly atmosphere in the laboratory and the good collaboration
- Especially my supervisors Dr. Helmut Neugebauer and Prof. Dr. N.S. Sariciftci for their great support and helpful advices
- The international collaborators who provided the materials, A. Dhanabalan and R. Janssen from the Eindhoven University of Technology, H. Meng and F. Wudl from the University of California, Los Angeles, N. Martin from the University of Madrid and J.C. Hummelen from the University of Groningen
- Dr. Johannes Theiner from the University of Vienna for providing the program S.C.A.D.A. and for his help in working with the program

Personally and specially I want to thank my family for their great financial and personal support during my studies and my girl friend for her personal support

*Thank You*

Eidesstattliche Erklärung:

Ich erkläre an Eides statt, dass ich die vorliegende Diplomarbeit selbständig und ohne fremde Hilfe verfasst, andere als die angegebenen Quellen und Hilfsmittel nicht benutzt bzw. die wörtlich oder sinngemäß entnommenen Stellen als solche kenntlich gemacht habe.

Linz, September 2002

David Mühlbacher

Die vorliegende Diplomarbeit entstand zwischen September 2001 und September 2002 am Forschungsinstitut für Organische Solarzellen der Technisch-Naturwissenschaftlichen Fakultät der Johannes Kepler Universität Linz unter Betreuung von Prof. Dr. N.S. Sariciftci und Dr. Helmut Neugebauer.

## **Abstract**

Low bandgap polymers are of great interest for the use in 'bulk heterojunction' solar cells to achieve higher power conversion efficiencies by better matching the solar spectrum and therefore a better exploitation of lower photon energies. To be able to predict the general usability of these materials for this purpose the HOMO and LUMO levels of the polymers have to fit into the energetic properties of a solar cell. In this work the electrochemical determination of the HOMO and LUMO levels of different materials and a comparison of the optical and the electrochemical band gap is presented.

The determination of the band edges and band gaps is done with cyclic voltammetry and electrochemical voltage spectroscopy of polymer films. The band gap obtained is compared with that from absorption spectroscopy.

In situ spectroelectrochemistry for both UV-VIS and IR is performed to support the results from the electrochemical measurements.

## **Zusammenfassung**

Polymere mit Bandlücken  $<1.8$  eV sind von großem Interesse um die Effizienz polymerbasierender Solarzellen durch effektiveres Einfangen des Sonnenlichts zu erhöhen. Um die grundsätzliche Verwendbarkeit dieser Materialien zu diesem Zweck vorhersagen zu können, müssen die Bandkanten für das HOMO und LUMO Energieniveau in das Energieschema einer Solarzelle passen. In dieser Arbeit wird die elektrochemische Bestimmung dieser Niveaus für verschiedene Materialien sowie ein Vergleich der optischen und der elektrochemischen Bandlückenwerte präsentiert.

Die Bestimmung der Bandkanten wurde mit Zyklovoltammetrie und elektrochemischer Spannungs-Spektroskopie durchgeführt. Die so erhaltene Bandlücke wird mit der aus der Absorptionsspektroskopie bestimmten verglichen.

In situ Spektroelektrochemie, sowohl mit UV-VIS als auch mit IR Licht, wird zur Unterstützung der vorhergehenden Ergebnisse verwendet.

# Table of Contents

<b>1</b>	<b>Introduction</b>	<b>5</b>
1.1	Motivation	5
1.2	Electrochemical Doping of conjugated polymers	8
1.2.1	The concept of doping as applied to conjugated polymers	8
1.2.2	Charges in conjugated polymers – solitons, polarons and bipolarons	10
1.2.3	Voltammetric behaviour of conjugated polymers	16
<b>2</b>	<b>Experimental</b>	<b>21</b>
2.1	Electrochemistry	21
2.1.1	Electrochemical voltage spectroscopy (EVS) and cyclic voltammetry (CV)	21
2.1.2	The microelectrochemical cell	24
2.1.3	In situ spectroelectrochemistry using IR and UV-VIS absorption	25
2.2	Spectroscopy	28
<b>3</b>	<b>Results and Discussion</b>	<b>29</b>
3.1	MDMO-PPV	29
3.2	PTPTB	38
3.3	PEDOT-EHI-ITN	46
3.4	PCBM and UCM-FG62	54
<b>4</b>	<b>Summary and Conclusion</b>	<b>57</b>
<b>5</b>	<b>References</b>	<b>61</b>
	<b>Curriculum vitae</b>	<b>67</b>
	<b>List of Publications</b>	<b>69</b>

# 1 Introduction

## 1.1 Motivation

The discovery of metal-like electrical conductivity of polyacetylene when exposed to oxidizing agents like iodine vapor in 1977 by Shirakawa together with Heeger and MacDiarmid opened a new field in the research of polymers [1-3]. For this discovery they were awarded the Nobel Prize for chemistry in 2000. The finding of this class of materials was very exciting, as they exhibit a unique combination of properties of metals and plastics such as electrical conductivity, optical activity, flexibility and easy processability [4-7]. Since that time, a lot of work and investigations were carried out on the synthesis of new conducting polymers and their properties for different applications. The list of investigated applications up to now reaches from batteries [8], smart windows [9], polymeric actuators [10] over transistors [11], sensors [12], photodiodes [13], lasers [14] to solar cells [15-19] and light-emitting diodes [20,21] (LED's).

Solar cells made of conjugated polymers are of special interest as the search for alternative energy sources is always going on. These devices, produced with thin film techniques, could have great advantages over their inorganic competitors due to much lower production costs and flexibility even if they do not reach the energy conversion efficiencies exceeding 24 % of inorganic materials [22], today.

In the 'bulk-heterojunction' organic solar cells with power conversion efficiencies up to 3 % blends of a poly[2-methoxy-5-(3',7'-dimethyloctyloxy)-1-4-phenylene vinylene], (MDMO-PPV) : 1-(3-methoxycarbonyl)-propyl-1-phenyl-(6,6)C<sub>61</sub> (PCBM) mixture are used [18,19]. However, MDMO-PPV has a bandgap of 2.2 eV and PCBM has a HOMO – LUMO transition of ~2 eV, thus the mixture absorbs between 300 and 600 nm. Fig. 1.1 shows the terrestrial solar spectrum, AM 1.5, and the total photon flux compared to the absorption spectrum of a MDMO-PPV/PCBM blend. The solar cells made of these materials can use only around 30 % of the total photon flux, as they do not absorb in the maximum region of the solar spectrum between 600 and 900 nm.

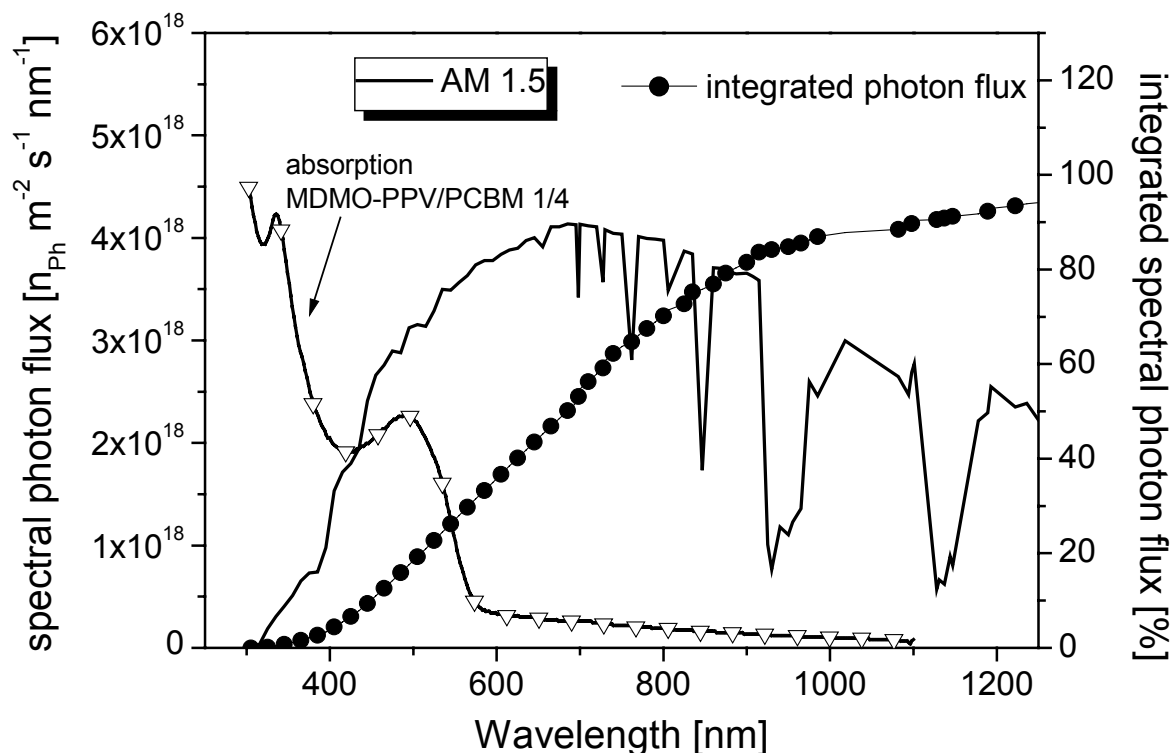


**Fig. 1.1:** Comparison of the terrestrial solar spectrum (—) and the integrated spectral photon flux (-●-) with the absorption of a MDMO-PPV : PCBM blend (-▽-) as the active layer in the ‘bulk-heterojunction’ solar cell

One way to achieve a better harvesting of the sunlight is the use of low-bandgap conjugated polymers with a bandgap of 1.8 eV or lower corresponding to an absorption down to 700 nm or lower. The absorption of such materials will match the solar spectrum better and can in that way enhance the efficiency of organic solar cells.

However, besides the width of the gap, which can be easily determined with absorption spectroscopy, also the energy levels of the valence band (VB) and the conduction band (CB) of the low-bandgap material have to fit into the energetic scheme of a photovoltaic device. Electrochemistry, and in special electrochemical voltage spectroscopy (EVS) [23-25] is a powerful tool to determine the energetic positions [26-31] of the edges of VB and CB in terms of eV vs. normal hydrogen electrode (NHE) level, since they correspond to the potential values for the onsets of oxidation and reduction in electrochemical reactions of conjugated polymers [32,33] as schematically shown in Fig. 1.2.

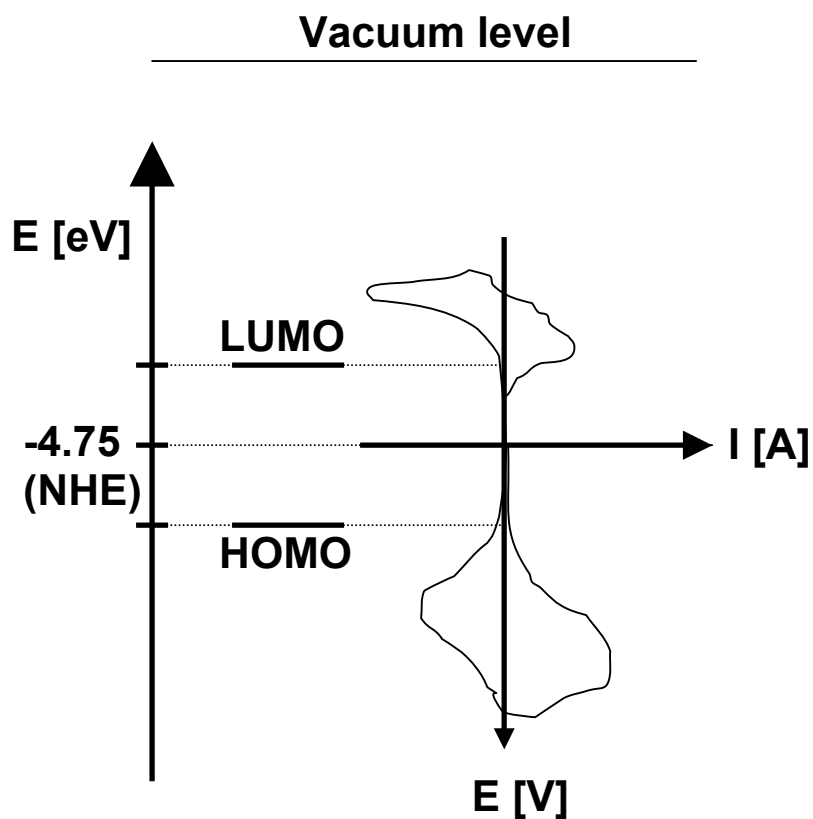


**Fig. 1.2:** Connection of Fermi energy scale and electrochemistry: the onset potentials for oxidation and reduction correspond to the HOMO and LUMO level

If the position of the normal hydrogen electrode (NHE) is known in the Fermi scale all other electrochemical potentials can easily be converted to this scale. Many different values for the NHE in the Fermi scale can be found in literature ranging from -4.31 to -4.85 eV [34-37]. For the determination of the band edges presented in this thesis a value of -4.75 eV for the NHE was chosen, because this value is well supported by photoelectron spectroscopic measurements [36,37 and references therein].

The aim of this work is to determine the energetic positions of the edges of the VB and the CB of low-bandgap polymers with electrochemistry to predict the energetic scheme for a photovoltaic device. A comparison of the optically and electrochemically determined values of the gap and spectroelectrochemical measurements are done to further consolidate the data. The results are compared with that of MDMO-PPV and PCBM as the reference materials for the use in organic solar cells.

## 1.2 Electrochemical Doping of conjugated polymers

The report of Shirakawa *et al.* [1-3] showed that the electrical conductivity of polyacetylene can be increased through reaction with an oxidative agent or electron acceptor (p-doping) or a reducing agent or electron donor (n-doping) by several orders of magnitude. The electronic properties of conjugated polymers can be described with molecular orbital theory [38] leading to the structural characteristics of a linear  $\pi$ -electron system [39-41].

These conjugated polymers contain electronic states [40-46] that can be reversibly emptied or filled with electrochemical techniques resulting in metal-insulator transitions, which has an enormous potential for wideranging practical applications [3,8-21]. Due to this fact electrochemistry of conjugated polymers is an actively investigated research field.

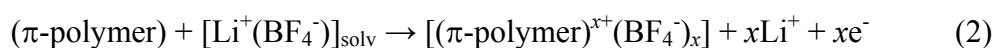
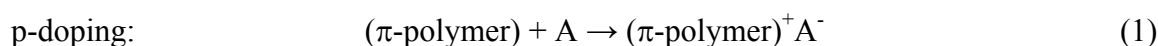
Electrochemistry is generally a powerful tool in the work with conjugated polymers. Besides the characterization of the materials with electrochemical methods, also electropolymerization by oxidation and also reduction as a way of synthesis can be applied for most of the important polymers [32,39,47-50].

### 1.2.1 The concept of doping as applied to conjugated polymers

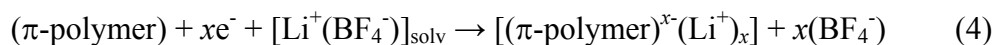
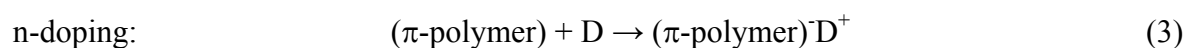
Chemically produced conjugated polymers are insulators after the cleaning steps. Their metal like properties, i.e. their high conductivity, arise only after 'doping', concomitant with a change of the redox state of the polymer. The term 'doping' is generally correct, as a small quantity of a dopant gives rise to disproportionally large changes of the properties of the material. Still its use implies similarities between the doping of organic and inorganic semiconductors, which is not the case.

In silicon, as an example for an inorganic semiconductor, the dopant occupies positions within the lattice of the host material. This results in an either electron-rich (i.e. phosphorus as dopant) or electron-deficient (i.e. boron as dopant) site, with no charge transfer taking place between the two species. The effect of doping is due to the amount of the valence electrons of the dopant and the host material. As silicon has four valence electrons, replacement with boron with only three valence electrons results in electron-deficiency, whereas doping with phosphorus with five valence electrons gives electron-rich sites.

In contrast to this, the doping of conjugated polymers [4,32,33,39] is essentially a charge transfer reaction that results in a partially oxidized or reduced polymer rather than the creation of holes or electrons. It can be done chemically with reducing (Donor D, n-doping) or oxidizing (Acceptor A, p-doping) agents or electrochemically by applying a certain voltage. Oxidation in this context is referred to as p-doping (again in analogy to inorganic semiconductors), the basic processes are shown in reactions (1) and (2) as examples for chemical and electrochemical doping, respectively.



As can be seen in both cases, for doping also a compensation of the generated charge is needed resulting in a 'poly-salt'. Similarly n-doping results in partial reduction of the polymer chain, as shown in reactions (3) for chemical doping and (4) for electrochemical doping.



Chemical and electrochemical doping generally gives similar results by means of the properties of the induced charges. The main advantage of electrochemical doping over the chemical way lies in the control of the doping level [51]. This can easily be done electrochemically via the applied voltage giving highly reproducible results, whereas with chemical doping attempts to reach intermediate doping levels often result in inhomogeneous doping.

## 1.2.2 Charges in conjugated polymers – solitons, polarons and bipolarons

### *General introduction*

In conjugated polymers with only carbon atoms two of the three p-orbitals of carbon are in the three  $sp^2$  hybrid orbitals [38]. Of these, two are used for the  $\sigma$  bonds of the polymer backbone, while the third forms a bond to hydrogen or any other substituent. The so far unused third p-orbital, the  $p_z$ -orbital, gives rise to an extended  $\pi$ -system along the chain, which gives conjugated polymers their unique properties [52-54]. The bond formation is depicted in Fig. 1.3 for the example of *trans*-polyacetylene.

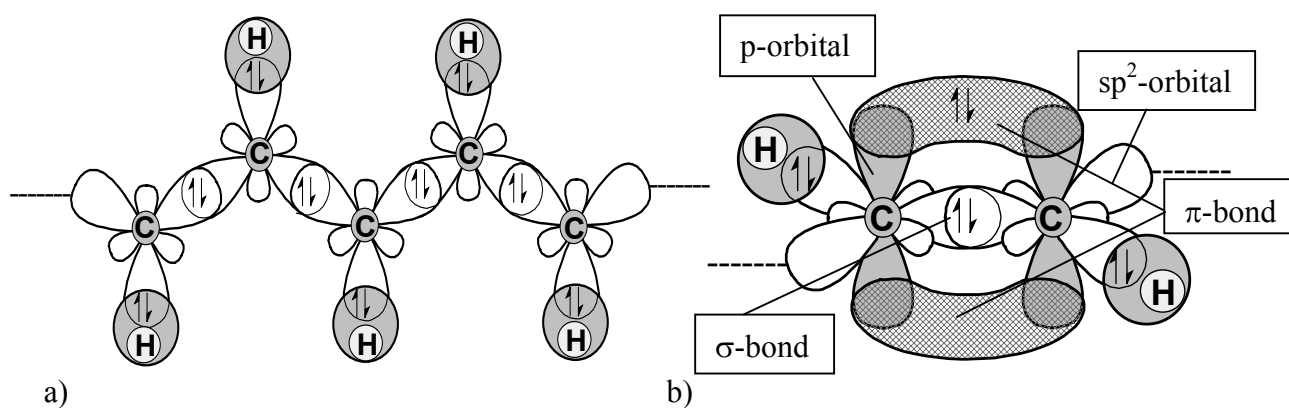


**Fig. 1.3:** a) Formation of  $\sigma$ -bonds in polyacetylene by overlapping of  $sp^2$ - (carbon) and  $1s$ - (hydrogen) orbitals; b) Formation of  $\pi$ -bonds through overlap from the side of the  $p_z$ -orbitals

Principally, this should give a metallic material with a half-filled conduction band if all bonds were of equal length. But due to the Peierls distortion [55] dimerization occurs that breaks the symmetry of the polymer chain. In this dimerized form the  $\pi$ -electrons are concentrated between alternate pairs of carbon atoms, which is consistent with the observation of alternation of double and single or shorter and longer bonds along the chain. The lowering of the symmetry takes place to minimize the ground state energy. Due to this lowering of the ground state the  $\pi$  orbital is split into a filled  $\pi$ -orbital (HOMO, valence band, bonding orbital) and an empty  $\pi^*$  orbital (LUMO, conduction band, antibonding orbital) with a certain energy gap between, the so called  $\pi$ - $\pi^*$  bandgap, which is characteristic for semiconducting materials and lies in the range of 1 to 4 eV for conjugated polymers and is an essential point for device applications.

This value of the band gap varies depending on several parameters and can be controlled to a certain extent chemically [56-61]. Equation (i) describes the band gap in the bulk as the sum of five contributions. Fig. 1.4 shows the structural meanings on the example of poly-*p*-phenylene.

$$E_g = E_{\Delta r} + E_{Res} + E_{\theta} + E_{Sub} + E_{int} \quad (i)$$

$E_{\Delta r}$  is the energy contribution of the bond length alternation,  $E_{Res}$  is the resonance stabilization energy,  $E_{\theta}$  the energy contribution caused by the inter ring torsion angle,  $E_{Sub}$  the influence of substituents and  $E_{int}$  the intermolecular or inter chain coupling in the solid state.

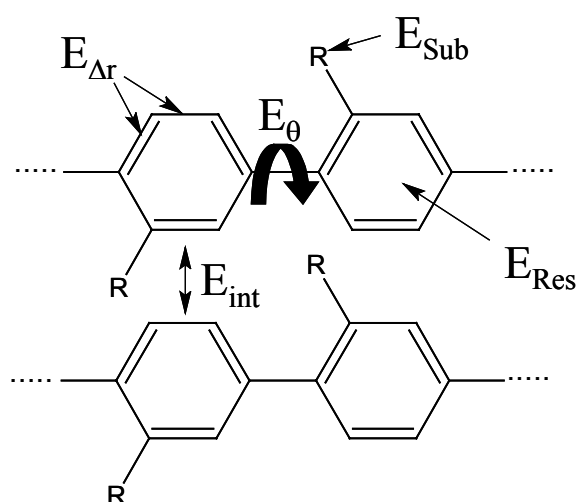


**Fig. 1.4:** The different parameters determining the bandgap of conjugated polymers in the solid state shown on the example of poly-*p*-phenylene: bond length alternation  $E_{\Delta r}$ , resonance energy  $E_{Res}$ , inter ring torsion angle  $E_{\theta}$ , substituent effects  $E_{Sub}$  and inter chain coupling  $E_{int}$

*Solitons:*

Trans-polyacetylene is a polymer with a degenerate ground state since the double and single bonds can be interchanged without changing the ground state energy. Therefore the ground state has two configurations A and B with the same energy as shown in Fig. 1.5 [40,41,45].

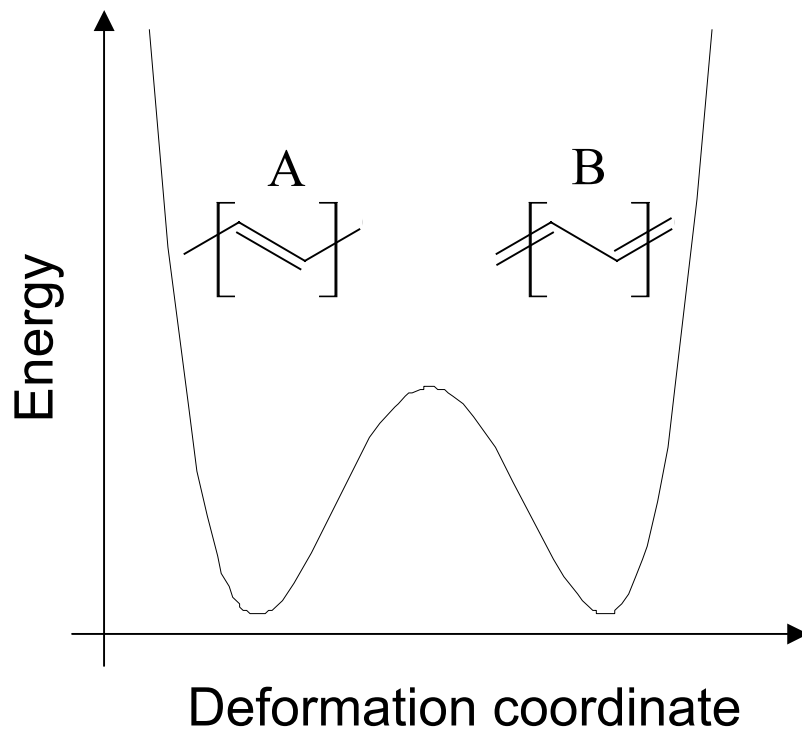


**Fig. 1.5:** Potential energy curve for trans-polyacetylene showing the two equivalent structures

If both of the energetically equivalent configurations coexist on the same chain a structural defect will occur at their interface. This defect is called a (neutral) soliton, it consists of a single unpaired electron that can extend over approximately ten carbon atoms [40-42]. One new localised electronic state is formed in the middle of the  $\pi$ - $\pi^*$  gap, which can accommodate up to two electrons. Doping adds or removes an electron to or from this state during n- or p-doping leading to a negatively or positively charged soliton, which can also be called spinless anion or cation. A band diagram for neutral, positive and negative soliton is shown in Fig. 1.6. Associated with these three types of solitons new optical transitions depending on their symmetry allowance can be observed in optical absorption spectra, which are indicated with dotted arrows in Fig. 1.6. Only transitions from levels with an odd parity to levels with an even parity in the wave function or vice versa are allowed. The parity of the wave function is alternating with every energetic level.

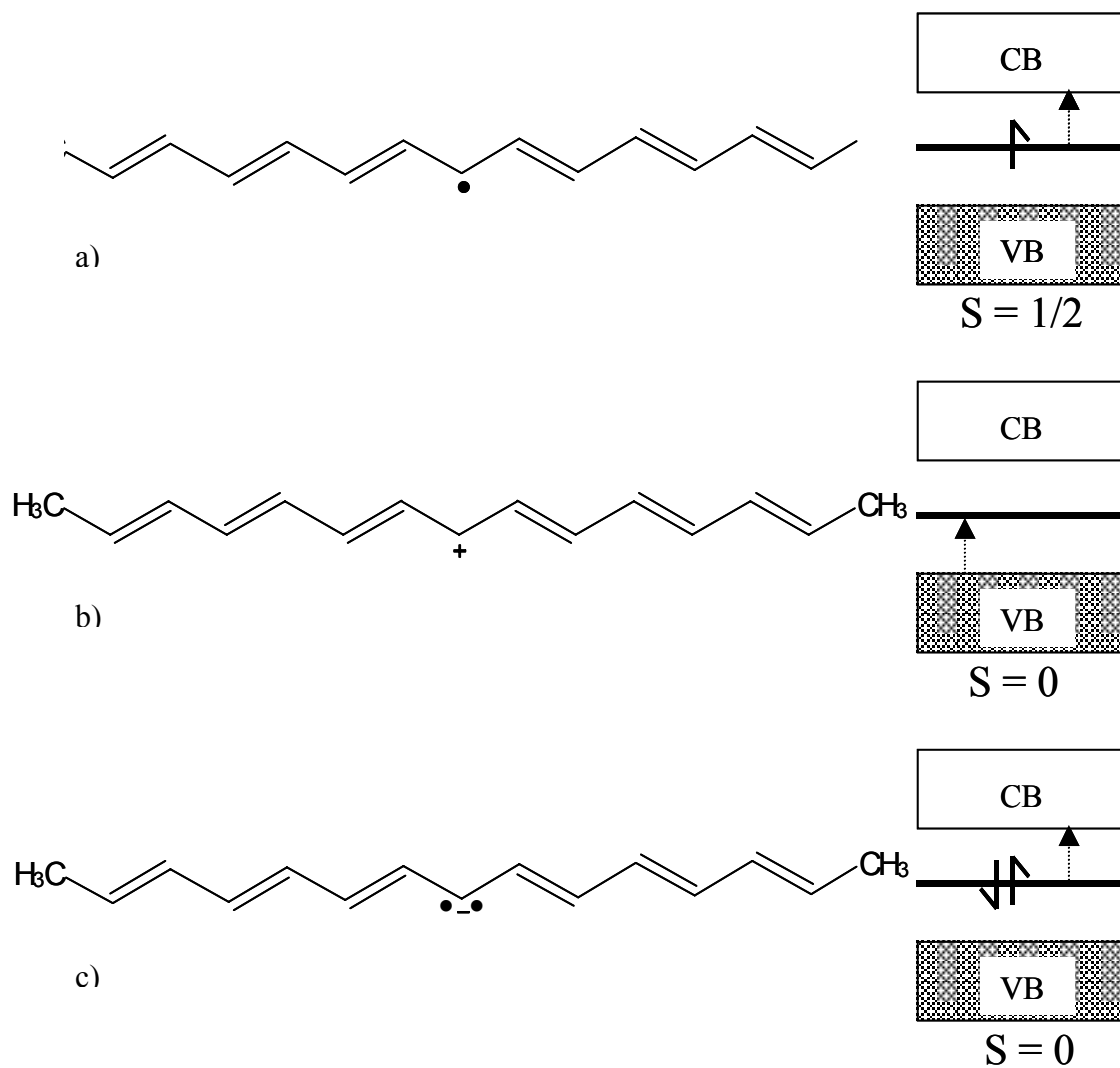


**Fig. 1.6:** Soliton structures in polyacetylene and corresponding electronic states in the band gap, a) neutral soliton, b) positive soliton, c) negative soliton; only the neutral soliton carries a spin ( $S$ ), dotted arrows indicate optical transitions to and from the mid-gap state

### *Polarons and bipolarons:*

Most other conjugated polymers have two energetically inequivalent bond alternation structures, which means they have a non-degenerate ground state [42-45]. For example in poly(*p*-phenylenevinylene) (structure is shown in Fig. 1.7) the quinoid structure (B) is less stabilized and therefore higher in energy than the benzenoid form (A). Fig. 1.7 shows the energy diagram for these two structures.

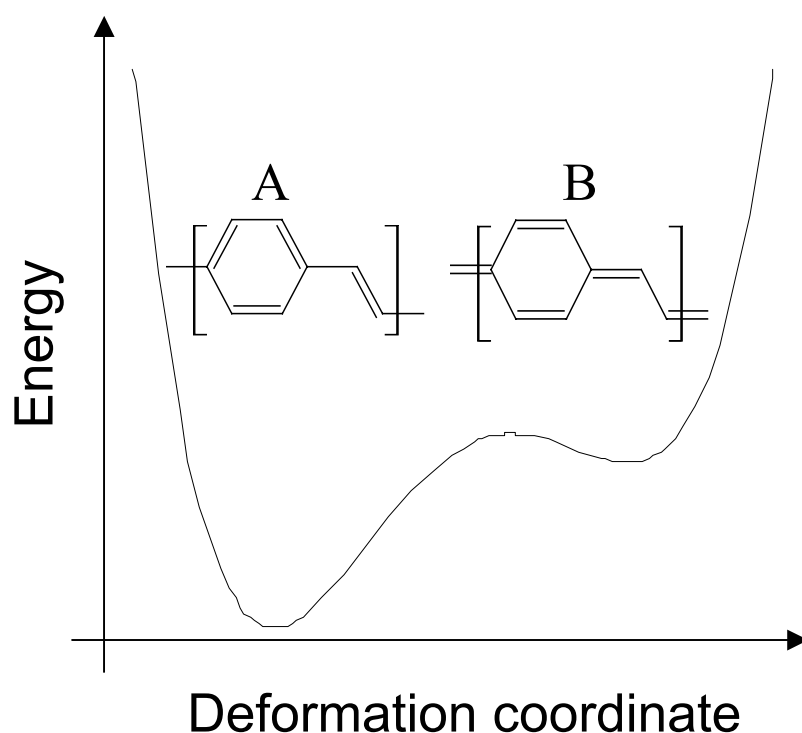


**Fig. 1.7:** Potential energy curve for poly(*p*-phenylenevinylene) with its energetically inequivalent structures, benzenoid (A) and quinoid (B)

A defect region will be created in the presence of charge carriers between uncharged benzenoid parts on the conjugated polymer. Upon p- or n-doping charge carriers called polarons (radical cation or anion) and bipolarons (spinless dication or dianion) are formed and two new electronic states are created in the  $\pi$ - $\pi^*$  band gap. A band scheme of the above described is given in Fig. 1.8. The dotted arrows indicate new possible optical transitions, depending whether they are allowed by symmetry or not. Only transitions from levels with an odd parity to levels with an even parity in the wave function or vice versa are allowed. The parity of the wave function is alternating with every energetic level.

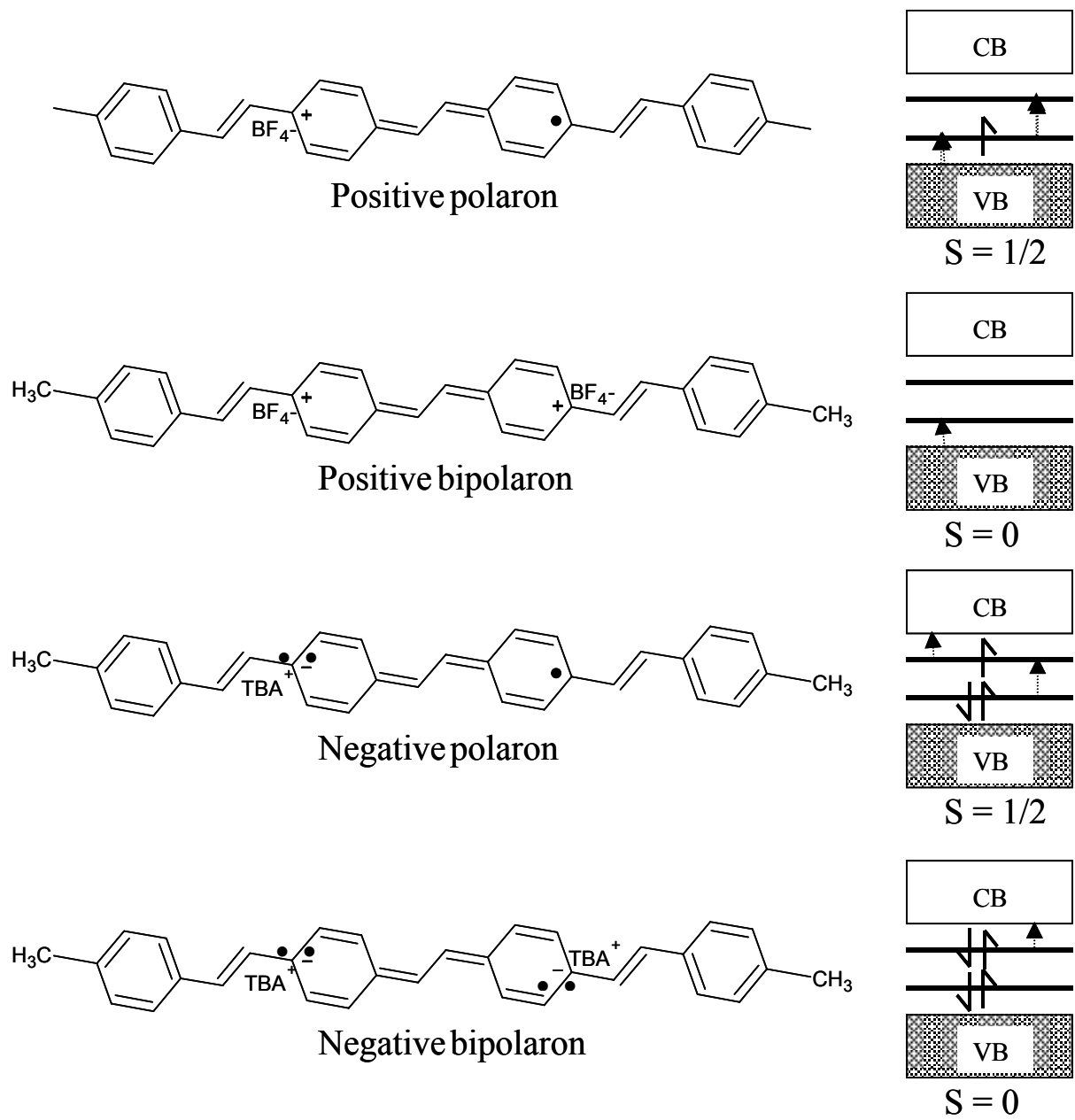


**Fig. 1.8:** Polaron and bipolaron structures in poly(*p*-phenylenevinylene) with their corresponding electronic states in the band gap; only positive and negative polaron carry a spin ( $S$ ), dotted arrows indicate possible optical transitions to and from the mid-gap states

Calculations show that the removal of an electron (p-doping) leads to the formation of a positive polaron (radical cation) whose associated quinoid geometry relaxation extends over three phenyl rings [62]. For removing a second electron from the polymer chain when doping proceeds two possibilities are given. The first possibility is that a second polaron will be created anywhere along the chain leading to two polarons. The second possibility is that the second electron is removed from the already existing polaron giving rise to a bipolaron. For both processes the formation energies are predicted to be roughly the same, but the ionisation energy for bipolaron formation should be substantially lower. Therefore one bipolaron is thought to be thermodynamically more stable than two coexisting polarons [45], despite the coulombic repulsion, which is screened to a large extent by the counterions near the charge carrier introduced upon chemical or electrochemical doping.

However, experimental findings attributed to bipolarons can in the same way be explained by using the concept of interchain polaron pair formation without any creation of bipolarons [63,64]. These are formed due to Coulomb interactions between a positive and a negative polaron on two neighboring chains also leading to no macroscopically detectable spin. Moreover, there has been no direct experimental proof for bipolarons yet.

The question which model better reflects the reality is not solved and the discussion is still controversial. For the interpretations given in this thesis only formation of polarons was taken into account.

### 1.2.3. Voltammetric behaviour of conjugated polymers

Under assumption of the ideal case with fast electron transfer across the polymer and a reasonable large concentration of mobile ions inside the polymer, one could anticipate from cyclic voltammetry of redoxactive films completely symmetrical and mirror-image cathodic and anodic waves [33,39], which is shown in Fig. 1.9. The peak potentials and current levels are identical and the current for this case is described through equations (ii) to (iv) [65-67].

$$i = \frac{n^2 F^2 A \Gamma_T v \cdot \exp \theta}{RT(1 + \exp \theta)^2} \quad (\text{ii})$$

with  $\theta = \frac{nF}{RT} \cdot (E - E^0)$  (iii)

and  $\Gamma_T = \Gamma_O + \Gamma_R$  (iv)

Equation (iv) corresponds to the total surface  $\Gamma_T$  covered with reduced ( $\Gamma_R$ ) and oxidized ( $\Gamma_O$ ) sites,  $n$  is the number of electrons taking part in the reaction,  $F$  is the Faraday constant,  $A$  is the the electrode area,  $v$  is the scan rate,  $\theta$  is the potential for the investigated reaction (see equation (iii)),  $R$  is the gas constant and  $T$  is the temperature.

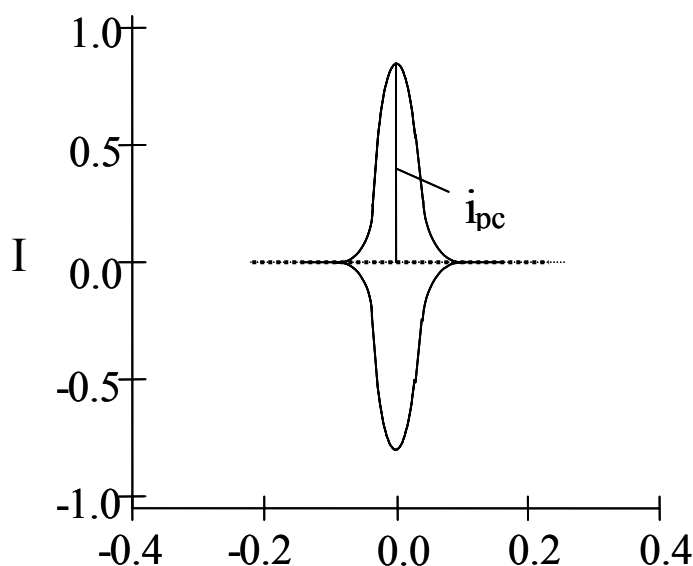


**Fig. 1.9:** Theoretical cyclic voltammogram for a redoxactive polymer film with non-interacting redox centres

Besides mirror symmetry of the waves also the current  $i$  and the scan rate  $v$  are directly proportional to each other, which is in contrast to dissolved redox systems. In reality, the waves are shifted in relation to each other and become increasingly asymmetrical [68-70]. This can be seen from Fig. 1.10, where a cyclic voltammogram of PTPTB (structure and full name in chapter 3.2) is shown.

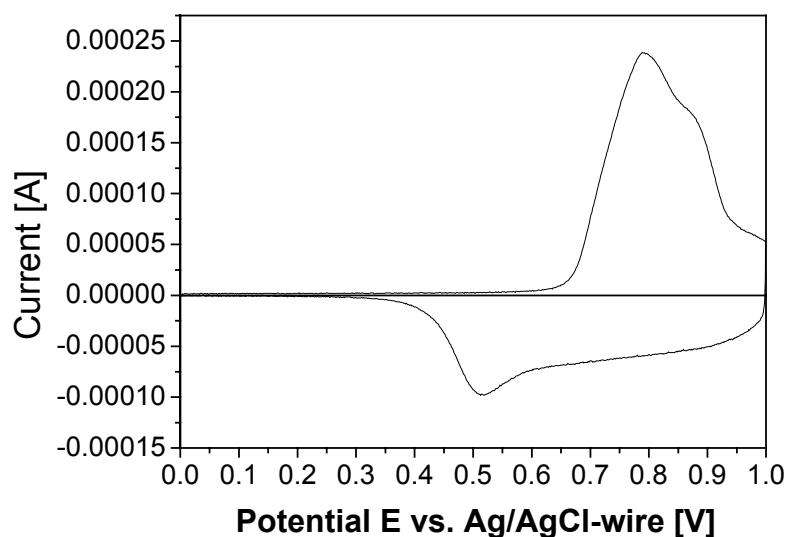


**Fig. 1.10:** Cyclic voltammogram of PTPTB dropcast onto a Pt electrode in  $\text{CH}_3\text{CN}/0.1 \text{ M TBAPF}_6$ , scan rate  $10 \text{ mV/s}$ ,  $E_{\text{Ferrocene}}^{1/2} = 445 \text{ mV}$

Two remarkable features can be seen from this plot. First, the anodic and the cathodic peaks are separated by  $260 \text{ mV}$ , which means in the common electrochemical sense that the redox reaction is 'irreversible'. Second, the steep, anodic wave is usually followed by a broad, flat plateau-like feature which also appears in the reverse scan as a capacity-like plateau before the cathodic wave, whose peak current has approximately half the value of the anodic peak.

The first explanation for these phenomena was made in terms of the simple theory for redox polymers as a kinetic effect of slow heterogeneous charge transfer, in which the interactions between the charged oligomeric segments were assumed to be negligible. The thermodynamic redox potential was calculated as the mean value between the peak potentials of the cathodic and the anodic wave [39, and references in there]. From the discrepancies of this theory it was concluded that the neutral polymer should have a conjugation length of 5 to 10 monomeric units. Quantum mechanical calculations also suggested that the onset potential reflects only the initial ionization of conjugated polymers while further ionization should lead to structural changes [39,71].

Based on this first assumption other concepts were developed to refine agreement with the experimental results, taking also structural changes in account. The fact that the peak separation is not essentially a function of the potential sweep rate suggests a chemical reaction following charge transfer [33, and references in there].

Upon oxidation the molecules stabilize themselves from the twisted benzenoid to the partially planar quinoid form in the case of aromatic polymers. Confirmation of this theory was found through work with the corresponding oligomers [33, and references in there]. In solution electrochemistry on oligomers gives reversible reactions, whereas when deposited as a film and the free rotation is hindered in the bulk, electrochemical irreversibility appears.

For the explanation of the constant current region, the question arises to what extent one can or must distinguish between faradaic and capacitive processes. In a first assumption only the anodic 'peak-shaped' wave was considered to be a faradaic process and the broad anodic tail was considered to be just an effect of the double layer capacity [39,72,73]. However, the results of the oligomer experiments mentioned above also can give a plausible explanation for this phenomenon [33], which does not take capacitive effects into account.

In the preparation of conjugated polymers often little attention is paid to the degree of polymerization, so that a mixture of oligomers and polymers with different chain lengths and probable cross linking is obtained. From Fig. 1.9 it appears that a number of redox potentials closely neighbored are effective in conjugated polymers. As these are distributed over a wide range of the electrode potential due to the different chain lengths, a typical cyclic voltammogram is a superposition of all these contributions. When the potential increases the accessible redox transitions decrease but stay finite within the experimental potential range, which may explain the plateau-like region following the peak of the anodic wave just in terms of faradaic contributions.

Still, truly irreversible electrochemistry is also well-known for conjugated polymers and may lead to cross linking, nucleophilic attack of the aromatic ring etc. and reduce the redox capacity of the polymers.

Electrochemical voltage spectroscopy (EVS) gives essentially the same information as obtained from cyclic voltammetry and shows also a hysteresis in charging and discharging [28] corresponding to the asymmetry of oxidation and reduction discussed for cyclic voltammetry. This technique will be described in detail in the following experimental chapter.

In this work the determination of the HOMO and LUMO levels as well as the band gap of different conjugated polymers by applying the methods of CV and EVS is presented. Optical absorption measurements are shown for comparison with and support of the electrochemically obtained value. In situ spectroelectrochemical techniques are presented as a good support and confirmation of the EVS measurements. The results are summarized comparing the materials with MDMO-PPV and PCBM as reference materials in the energy scheme of an organic solar cell.

# Experimental

## 2.1 Electrochemistry

All electrochemical experiments were carried out at room temperature in a glovebox under argon atmosphere except for in situ IR measurements. The supporting electrolyte was tetrabutylammoniumhexafluorophosphate (TBAPF<sub>6</sub>) 98% (Aldrich) in acetonitrile anhydrous (Aldrich). For cyclic voltammetry (CV) and EVS the working electrode (WE) as well as the counter electrode (CE) were platinum foils. The CE was put in a separate compartment with a ceramic frit for electrical contact. Polymer films were dropcast from toluene or chloroform (anhydrous, Aldrich) solutions (1/2 wt%) onto the WE using approximately 15 to 20  $\mu$ l solution. The Pt electrodes were cleaned from residual electrolyte or polymer before each use in the flame of a Bunsen burner. As a reference electrode (RE) a silver wire coated with AgCl was used inside its own compartment filled with the respective electrolyte ('quasi reference electrode' denoted later as Ag/AgCl-wire). Electrical contact was assured via a Vycor<sup>®</sup> tip purchased from Bioanalytical Systems, West Lafayette, Indiana. After each measurement the RE was calibrated with ferrocene ( $E^0 = 400$  mV vs. NHE, calibration mentioned in the figure captions). For all measurements a Jaissle 1002 T-NC potentiostat was used, which was controlled with a PC. The software used on the PC for controlling the potentiostat and data recording at the same time was S.C.A.D.A., which was developed at the University of Vienna.

Measurements with the microelectrochemical cell [69] were done on solutions of C<sub>60</sub> derivatives. The solvent for the electrolyte and the material was a 1 : 4 vol% mixture of acetonitrile and *o*-dichlorobenzene (ODCB) (both anhydrous from Aldrich).

### 2.1.1 Electrochemical voltage spectroscopy (EVS) and cyclic voltammetry (CV)

The setup used for EVS and CV was the same and is depicted in Fig. 2.1. CV is a dynamic method and was done on polymer films with a potential sweep rate of 10 mV/s between two limit potential values. The current that passes through the electrochemical cell is measured between the WE and the CE. CV was used to determine the interesting potential ranges for the later EVS experiments.

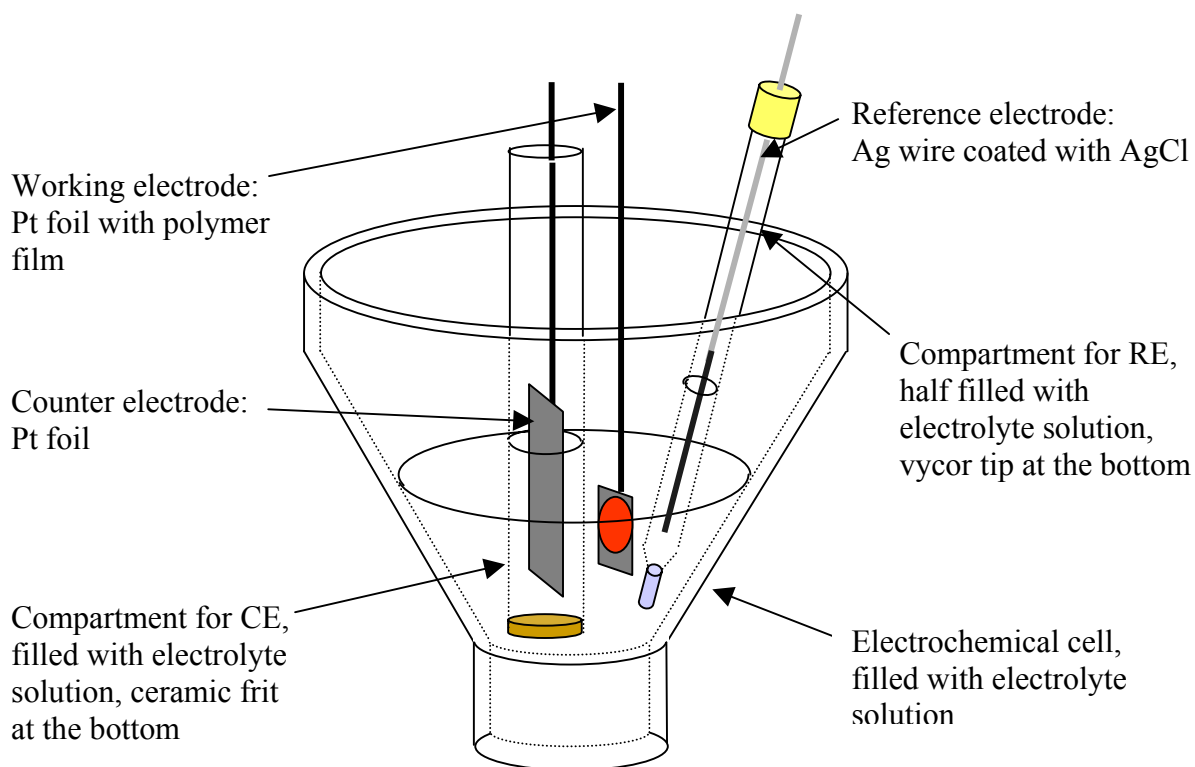


**Fig. 2.1:** Scheme of the electrochemical cell used routinely for CV and EVS measurements

The EVS method was developed to accurately measure charge/potential relationships under quasi-equilibrium conditions [23,32], the principle of EVS is shown in Fig. 2.2. It was used to determine the onsets of the oxidation and reduction peaks to get the energy values vs. vacuum level for the HOMO and the LUMO of the polymers.

Initially the system is allowed to reach equilibrium at the starting potential  $V$ . Under computer control the potential is then stepped to a new value  $V + dV$  (Fig. 2.2a) and the subsequent flow of current is monitored and recorded, while the system reaches its new equilibrium state (Fig. 2.2b). After a certain time for equilibration the potential is stepped to  $V + 2dV$  and the process is repeated. For the measurements herein reaching of the equilibrium was controlled with the waiting time after each step (another possibility that was not available so far is the use of a threshold current, below which the system is considered in equilibrium). The potential is stepped in this way to some maximum value and back to the initial point. After integration of the current during each step over time values of  $\Delta Q$  are obtained, which express the amount of accumulated charge during each potential step. The plot of  $\Delta Q/\Delta E$  vs.  $E$  (Fig. 2.2c) can then be interpreted as an 'infinitesimally slow' CV.

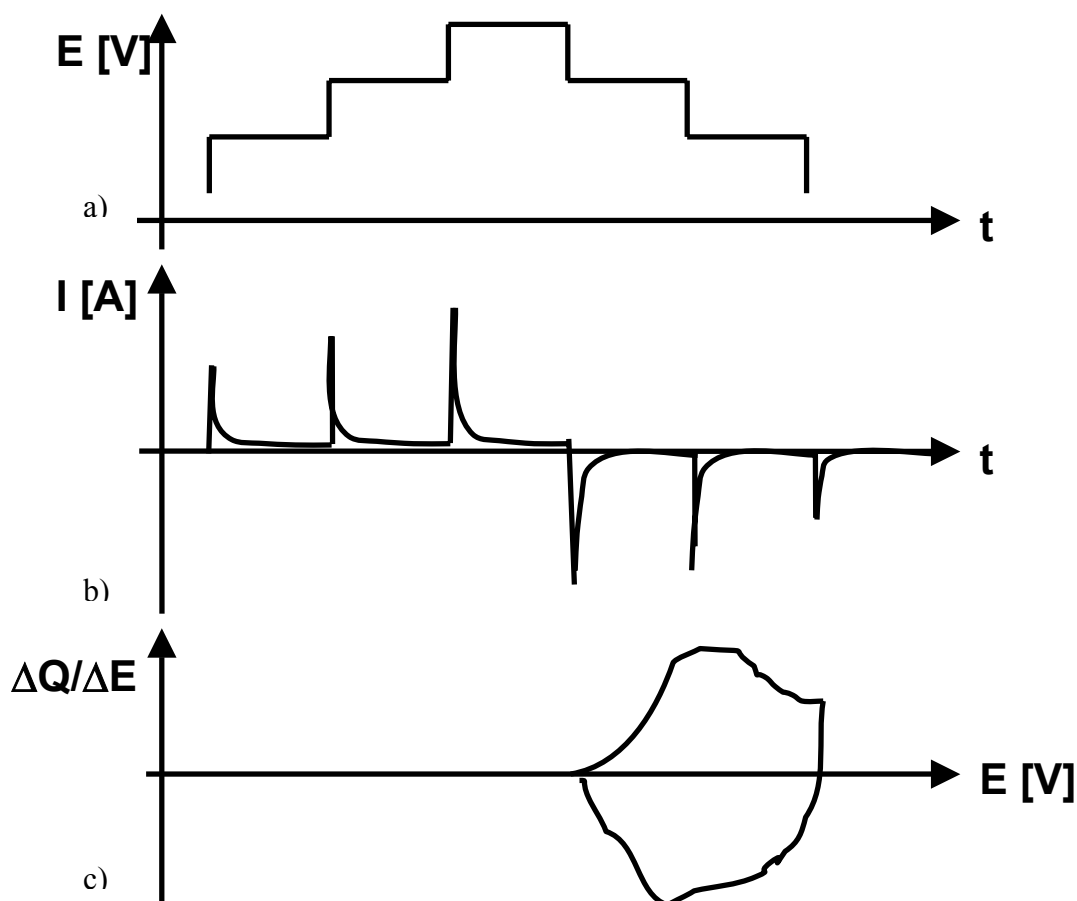


**Fig. 2.2:** Principle of electrochemical voltage spectroscopy: a) potential program, b) corresponding recorded current decay and c) plot of  $\Delta Q/\Delta E$  vs.  $E$  after integration

With S.C.A.D.A. a potential program was created with 10 mV steps in a suitable potential range for the onset of each polymer, which was determined from previous CV measurements. The time to wait after each potential step was chosen with 1 minute. Within this time the system was assumed to reach equilibrium easily.

For the integration of each step then a threshold value for the current of 1  $\mu\text{A}$  was chosen, which was taken from literature [23-31]. It was considered that oxidation or reduction starts, when the initial peak current as shown in Fig. 2.2b) reached 1  $\mu\text{A}$  relative to the baseline. This threshold value turned out to be very practical as below this value no well defined integration was possible due to the bad signal to noise ratio for these small values. The mistake that was made was only in the range of around 40 mV at a maximum and would not affect the determined values greatly.

### 2.1.2 The microelectrochemical cell

The work place with the microelectrochemical cell [74] for CV solution measurements with very small amounts of material was set up inside a glovebox as part of the work for the diploma thesis. It was initially designed for solution electrochemistry of  $C_{60}$  and derivatives because of their high costs but can be used for any material which is short on supply. A schematic picture of the setup is shown in Fig. 2.3.

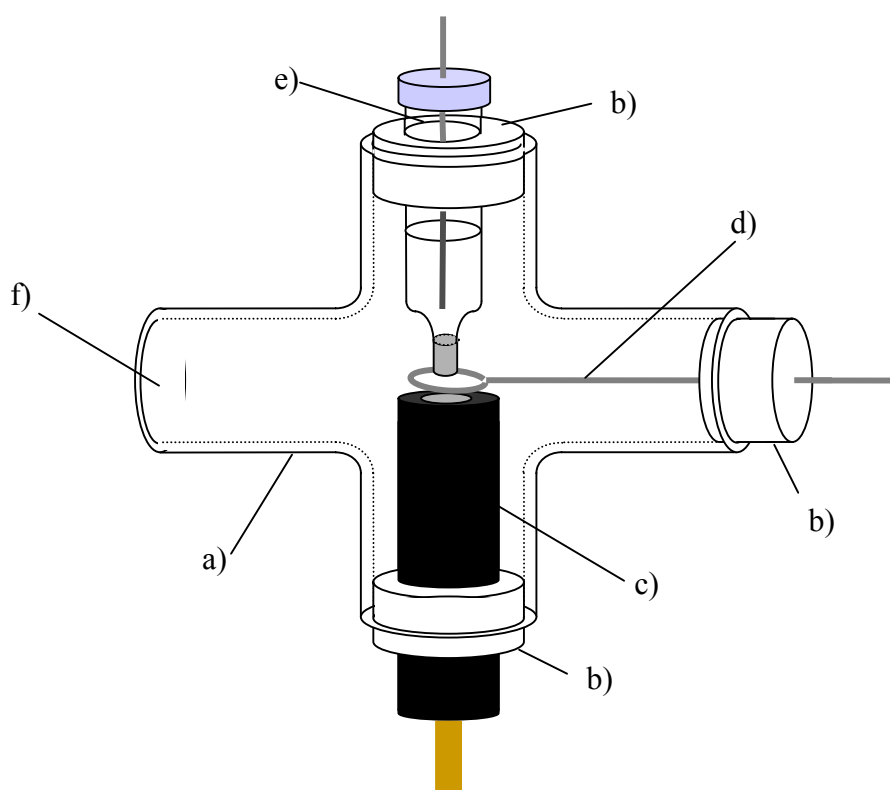


**Fig. 2.3:** Scheme of the microelectrochemical cell: a) glass cross with 4 female 14/20 ground-glass joints; b) Teflon<sup>®</sup> stoppers; c) working electrode, Pt disk with insulating coating; d) counter electrode, Pt wire in a loop; e) reference electrode, Ag wire coated with AgCl in glass tube filled with electrolyte and Vycor<sup>®</sup> tip at the bottom; f) unused opening for filling of the cell with a syringe

All three electrodes are of standard size and were purchased from Bioanalytical Systems, West Lafayette, Indiana. The Pt disk electrode as the WE is inserted from the bottom, the CE is a Pt wire is fixed as such that the loop sits above the WE. A non-aqueous Ag/Ag<sup>+</sup> quasi-RE, as described in the chapter before, is placed through the top opening above the other two electrodes. All electrodes are held in place by selfmade Teflon<sup>®</sup> stoppers.

The sample solution with the supporting electrolyte (0.1 M TBAPF<sub>6</sub>) and the analyte dissolved were brought inside with a Hamilton<sup>®</sup> syringe. Around 40 µl were enough to form a meniscus that covers all three electrodes. The remaining cell opening was closed with a full Teflon stopper to eliminate solvent evaporation during the measurement.

CV measurements were carried out from the solutions with a potential sweep rate of 50 mV/s. The electrochemical experiments were controlled from outside the glovebox with the computer and the S.C.A.D.A. software. After each measurement the analyte solution was exchanged to an electrolyte solution with ferrocene for calibration of the RE. The cleaning of the WE was done by polishing with diamond paste, first with a particle size of 1 µm and then with a size of 0.25 µm. The CE was cleaned in the flame of a Bunsen burner.

### 2.1.3 In situ spectroelectrochemistry using IR and UV-VIS absorption

With in situ spectroelectrochemistry the possible optical transitions mentioned in the discussion of charge carriers in conjugated polymers can be recorded using visible and infrared light. This is done at the same time as electrochemistry is performed and is therefore called 'in situ'. Absorption features of the neutral polymer chain are bleached for the benefit of the polaronic transitions in this case rising markedly red shifted of the initial band. The start of the bleaching of the main absorption band in the visible spectrum gives additional confirmation of the onset values determined with EVS.

In situ IR spectroelectrochemistry shows another polaronic transition in the NIR/MIR region. Additionally, new characteristic vibrational modes, the so called infrared active vibration (IRAV) modes [75-79], appear. The Raman active  $A_g$  modes in the pristine polymer become IR active due to the local breaking of the symmetry around the charge carrier. The high intensity of the IRAV bands originates from the large variation of the dipole momentum associated with the oscillation of the charged defect.

For in situ spectroelectrochemistry also 0.1 M TBAPF<sub>6</sub> in acetonitrile anhydrous was used as the supporting electrolyte.

### *In situ UV-VIS spectroelectrochemistry*

The construction of the in situ UV-VIS spectroelectrochemistry measuring setup was also part of the work for the diploma thesis. It was performed in a quartz cuvette as the electrochemical cell with 1 cm path length inside a glovebox. For the absorption measurements an Avantes AVS-USB2000 fiberoptic spectrometer in combination with an Avantes HL-2000 tungsten halogen light source was used.

Via an USB interface the spectrometer was connected to a computer and the measurements could be followed online with the provided software. The lamp was used inside the glovebox and with an optical fibre that was led into the glovebox the light could be detected. A scheme of the setup is depicted in Fig. 2.4.

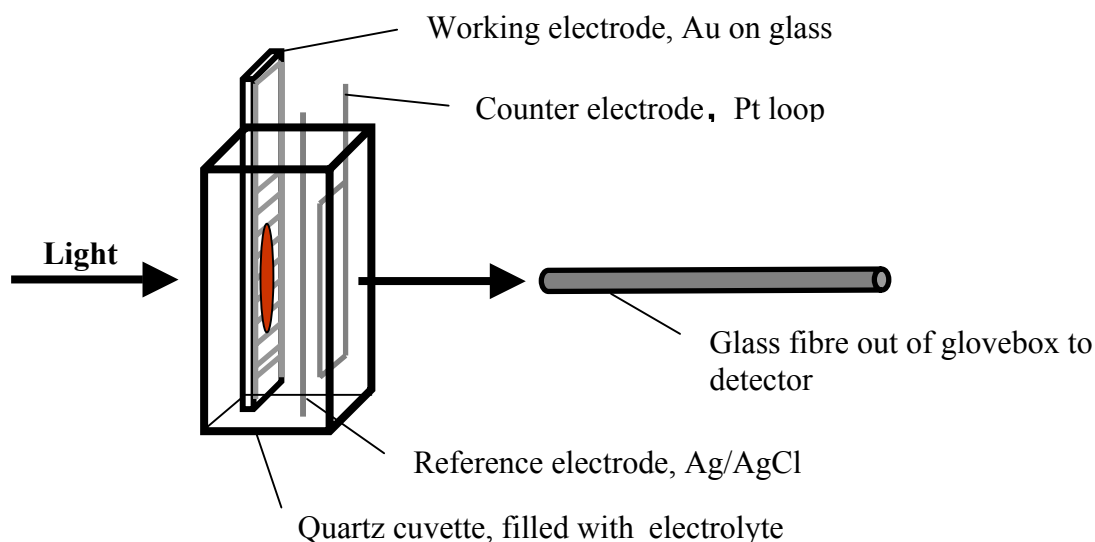


**Fig. 2.4:** Experimental setup for in situ UV-VIS spectroelectrochemistry

The WE was an evaporated Au grid on a glass plate, which was cleaned before in acetone and isopropanole using an ultrasonic bath. Evaporation was performed at a pressure of  $8 \times 10^{-6}$  mbar, 60 nm Au were evaporated. The polymer film was dropcast from solution onto the WE. The CE was a properly formed Pt wire, the quasi-RE a Ag wire coated with AgCl. Cleaning of the CE was done as mentioned before. A once used WE could not be cleaned properly from residual polymer as the evaporated Au does not cling to glass strongly and was at least partially removed during cleaning. For this reason a new WE was used for each measurement.

The whole electrochemical setup was put in the light path from the lamp to the spectrometer. In case of CV measurements with a potential sweep rate of 10 mV/s spectra were recorded every 5 seconds corresponding to snapshot spectra every 50 mV.

Also the EVS method was done with this setup. In this case the potential was adjusted by hand and spectra were recorded as soon as equilibrium conditions were reached, i.e. the current reached a steady value and no more changes of the online spectrum could be observed.

### *In situ IR spectroelectrochemistry*

In situ IR spectroelectrochemistry was performed with a Bruker IFS 66/S FTIR spectrometer in attenuated total reflection (ATR) geometry [80-83]. It was done on the regular measuring station and a scheme of this setup is shown in Fig. 2.5.

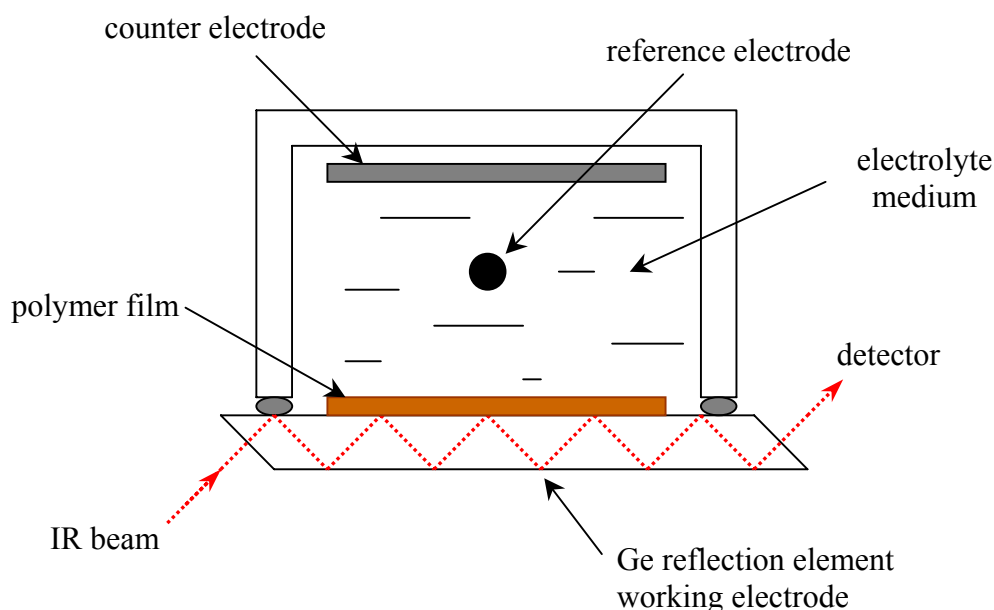


**Fig. 2.5:** Experimental setup for in situ IR spectroelectrochemistry performed in the ATR geometry

The central part of this method is a slightly n-doped Ge reflection element which acts as a waveguide for the IR beam and as the WE. Although the IR beam is totally reflected at the top and the bottom of the Ge element it can 'see' a small distance behind its barrier due to the phenomenon of the evanescent wave occurring under the conditions of total reflection.

Therefore changes of the IR spectrum of the polymer film deposited on top of the Ge element can be detected. The Ge element was cleaned before the measurements by polishing consecutively with a 1  $\mu\text{m}$  and a 0.25  $\mu\text{m}$  diamond paste and then rinsing with distilled water and acetone.

The CE electrode was a Pt foil, the RE the same as for UV-VIS spectroelectrochemistry. Measurements were performed in EVS mode similar as explained for UV-VIS spectroelectrochemistry. The spectra were related to a reference spectrum taken just before the investigated process and were calculated as  $\Delta(-\log T_{\text{ATR}})$ , where  $T_{\text{ATR}}$  is the transmittance in the ATR geometry.

## 2.2 Spectroscopy

Absorption measurements on dropcast films were carried out both at room temperature and after cooling with liquid He. For cooling an Oxford Instruments cryostat was used. The absorption measurements were performed with the Avantes AVS-USB2000 fiberoptic spectrometer. The optical bandgap was determined as the crossing point of a tangential through the turning point of the low energy side of the spectrum and the lengthened baseline for each substance.

Photoluminescence was measured also on dropcast films using a homemade setup also used for photoinduced absorption (PIA) measurements. The sample was excited with an argon laser beam (488 nm) mechanically chopped connected to a lock in amplifier. The luminescence was measured in backscattering geometry with a silicon detector also connected to the lock in amplifier.

### 3 Results and Discussion

#### 3.1 MDMO-PPV

Poly[2-methoxy-5-(3',7'-dimethyloctyloxy)-1-4-phenylene vinylene] (MDMO-PPV) was measured to obtain reference data for the understanding of suitability of the other investigated materials for photovoltaic devices. It was purchased from COVION, the structure is shown in Fig. 3.1.

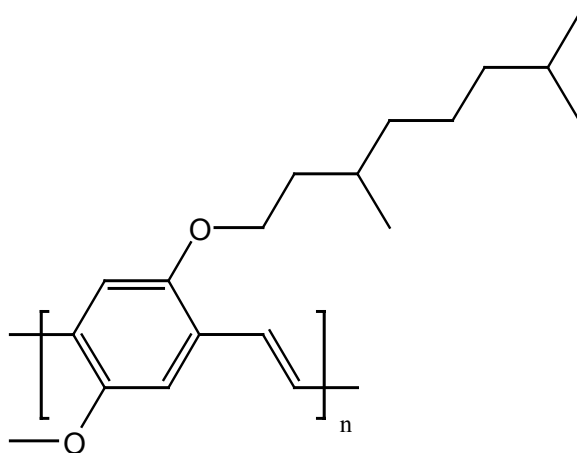


**Fig. 3.1:** Chemical structure of poly[2-methoxy-5-(3',7'-dimethyloctyloxy)-1-4-phenylene vinylene], MDMO-PPV

#### *Electrochemistry*

Fig. 3.2 shows a CV of MDMO-PPV. From this measurement the probable onsets for oxidation and reduction were estimated to be around +0.5 V and -1.8 V, respectively. The exact determination of the onsets was done with EVS. Fig. 3.3 and Fig. 3.4 show the EVS data for MDMO-PPV. For both oxidative and reductive direction multiple subsequent scans on freshly prepared films were performed to see the influence of the history of the investigated sample on the onset potential and generally on the redox behaviour. Oxidation was done two times followed by a reduction, again oxidation and reduction, and vice versa for reduction.

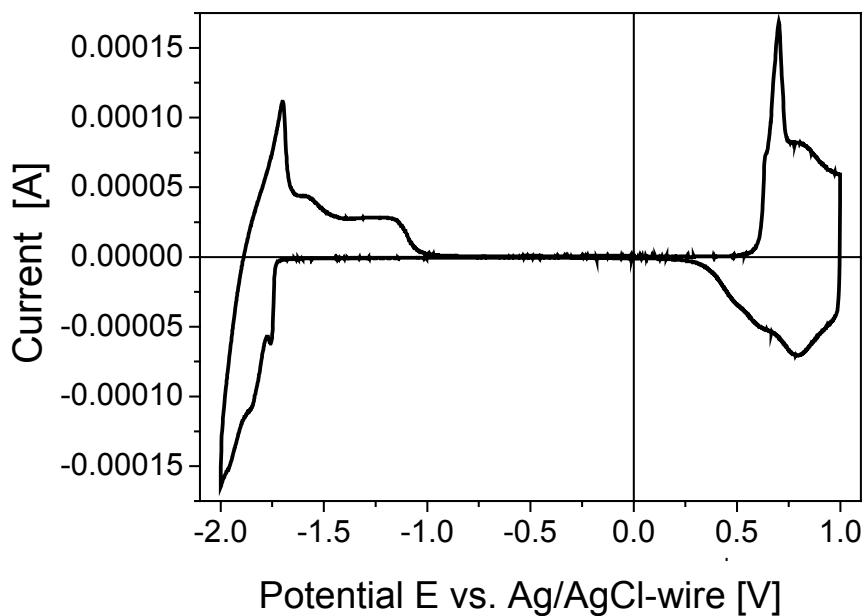


**Fig. 3.2:** Cyclic voltammogram of a MDMO-PPV film, scan rate 10 mV/s,  $E_{\text{Ferrocene}}^{1/2} = 420 \text{ mV}$

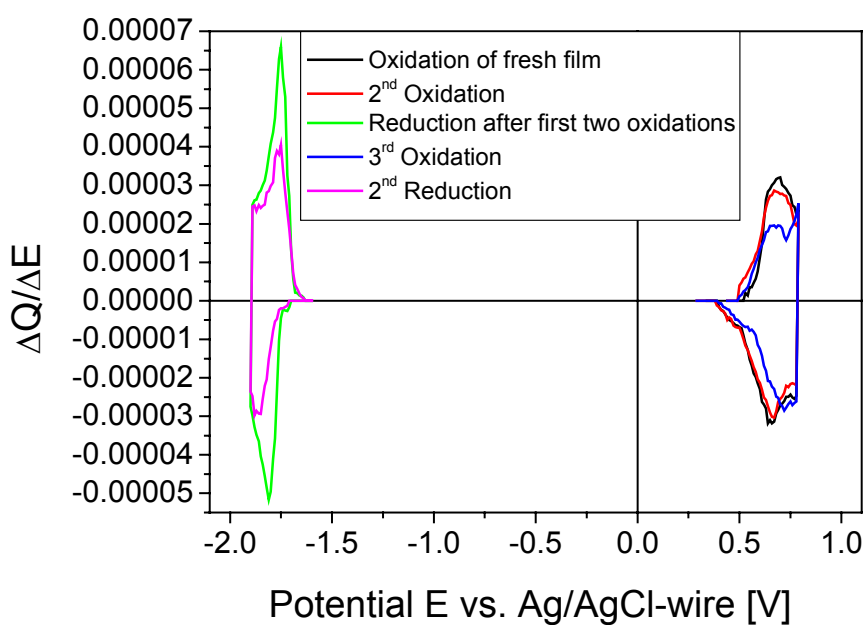


**Fig. 3.3:** EVS measurement for oxidation of MDMO-PPV with subsequent cycles presented in different colours as described in the legend,  $E_{\text{Ferrocene}}^{1/2} = +420 \text{ mV}$ ; the onset determined from the first oxidation was determined at +510 mV vs. NHE

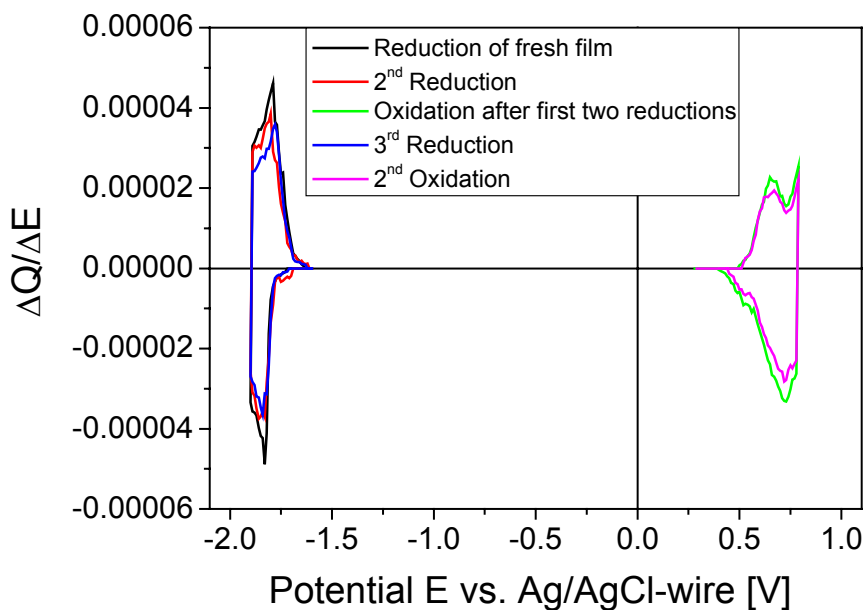


**Fig. 3.4:** EVS measurement for reduction of MDMO-PPV with subsequent cycles presented in different colours as described in the legend,  $E^{1/2}_{\text{Ferrocene}} = +420 \text{ mV}$ ; the onset determined from the first reduction was determined at  $-1750 \text{ mV}$  vs. NHE

The onset values for oxidation and reduction were determined at  $+510 \text{ mV}$  and  $-1750 \text{ mV}$  vs. NHE, respectively. This leads to an electrochemical bandgap  $E_g^{\text{EC}}$  of  $2.3 \text{ eV}$ . Assuming a value of  $-4.75 \text{ eV}$  vs. vacuum level for the NHE, the band edges for the HOMO and the LUMO can be estimated at  $-5.3 \text{ eV}$  and  $-3 \text{ eV}$ . Furthermore, only small changes depending on the history of the sample with variations of  $\pm 20 \text{ mV}$  for the onset potentials and small shifts of the anodic and cathodic waves could be found. The changes in the height of the peaks are more significant. Generally the shape of the anodic wave is altered if reduction was performed precedently, while the effect of preceding oxidation on the cathodic wave is rather small.

Fig. 3.5 shows the optical absorption and photoluminescence of MDMO-PPV. Unfortunately the He cryostat started leaking during the absorption measurement, so that cooling had to be stopped just below 110 K and the cryostat had to be defrosted. Therefore no absorption spectra could be obtained at lower temperature except for the measurement of PTPTB (see next chapter) and also photoluminescence measurements could only be carried out at room temperature.

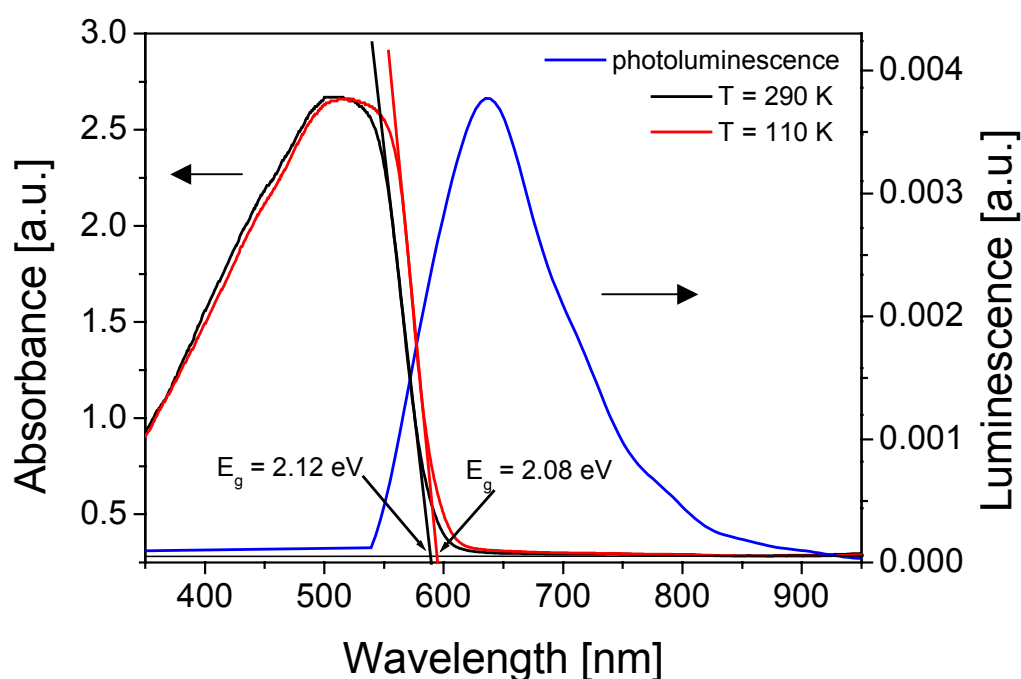


**Fig. 3.5:** Optical absorption and luminescence in the visible region of MDMO-PPV; black line shows the spectrum at room temperature, red line at 110 K, blue line shows the photoluminescence at room temperature (excitation at 488 nm)

The determination of the optical bandgap  $E_g^{\text{opt}}$  leads to a value of 2.1 eV with only a very small dependency on the temperature. This value is in close agreement with the electrochemical value of 2.3 eV. The photoluminescence spectrum looks as expected [84,85] for a PPV derivative.

A possible explanation for the changes of the spectrum itself, a small redshift and a very small change in the peak height, could be that at lower temperature the mean conjugation length of the conjugated segments is enlarged due to a more planar conformation along the chain.

Fig. 3.6 shows spectra of MDMO-PPV obtained during p- and n-doping with EVS. The potential was controlled by hand on the potentiostat with 10 mV steps and spectra were taken after equilibration of the system at the new potential.

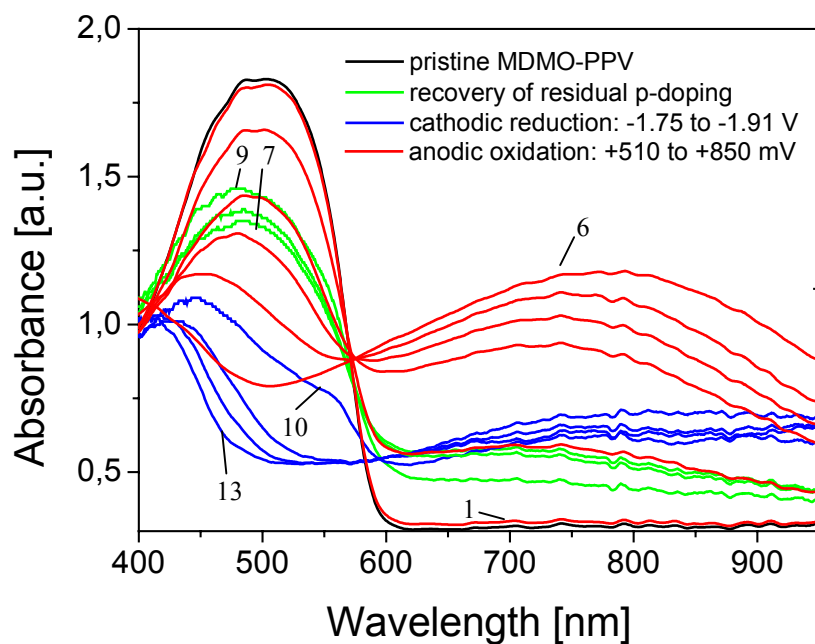


**Fig. 3.6:** In situ UV-VIS spectroelectrochemistry of p- and n-doping of MDMO-PPV: black line pristine polymer; oxidation as red lines from 1 to 6 (+510 to +850 mV vs. NHE); residual p-doping and partial recovery of pristine material as green lines from 7 to 9 (0 to  $-1.73$  V vs. NHE); reduction as blue lines from 10 to 13 ( $-1.75$  to  $-1.91$  V)

The main absorption band is bleached upon doping and a new broad band in the red to near infrared region is evolving upon p- and n-doping (red and blue set of lines in Fig. 6). This band is due to one of the new polaronic electronic transitions induced upon doping. P-doping of MDMO-PPV is not completely reversible but the polymer recovers to a certain extent while going to more negative potentials or with time (green set of lines in Fig. 6). N-doping is differently shaped and not so strong bands and is also not completely reversible.

With this technique the onset potentials of EVS were confirmed. Bleaching of the ground state transition starts at potentials determined with EVS, supporting these values.

Similar information except for the clearly determined onset potentials can be obtained from taking spectra periodically during CV scans. Fig. 3.7 shows the changes of the absorbance of MDMO-PPV related to the pristine material during an oxidative and a reductive cycle taken consecutively on the same polymer film.

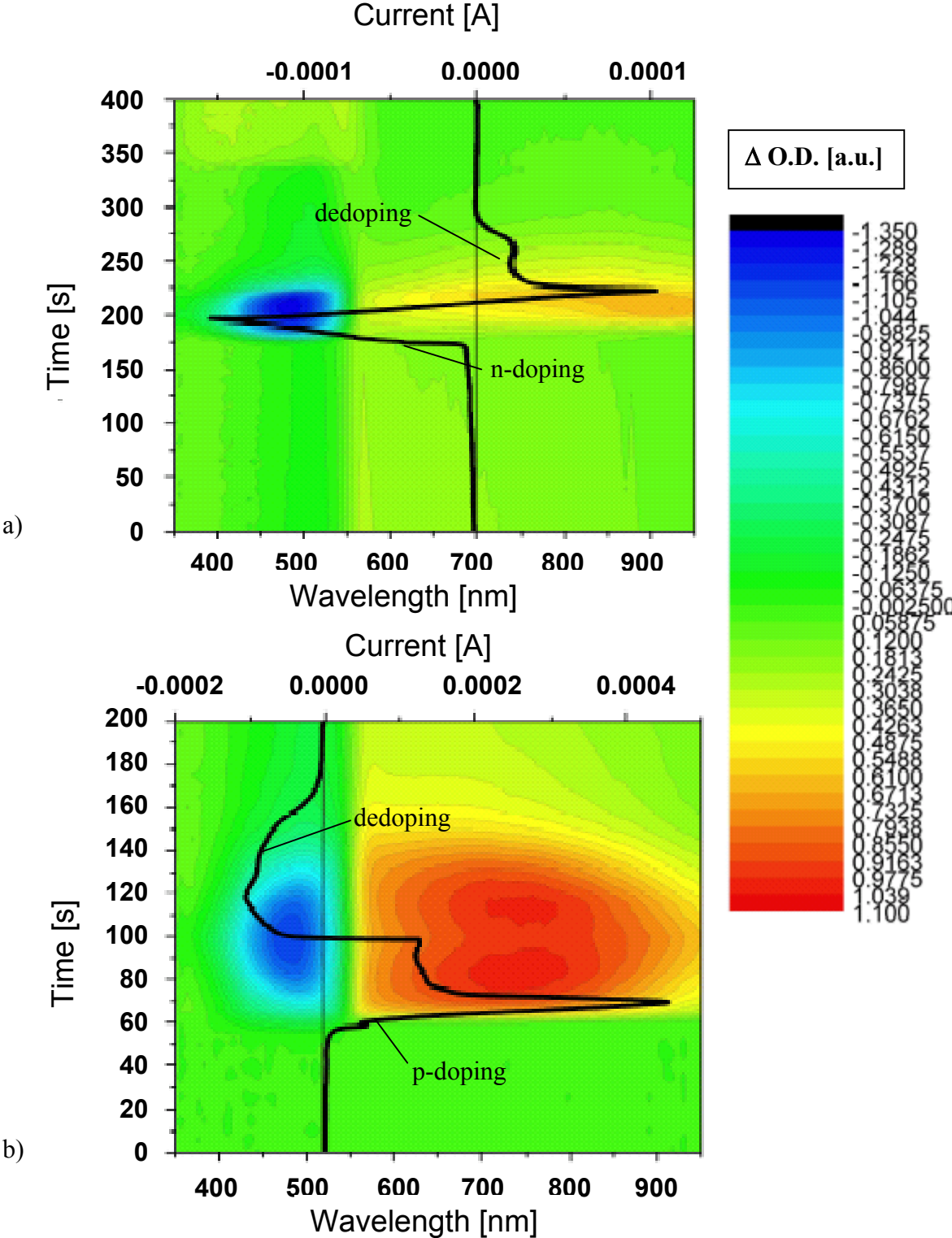
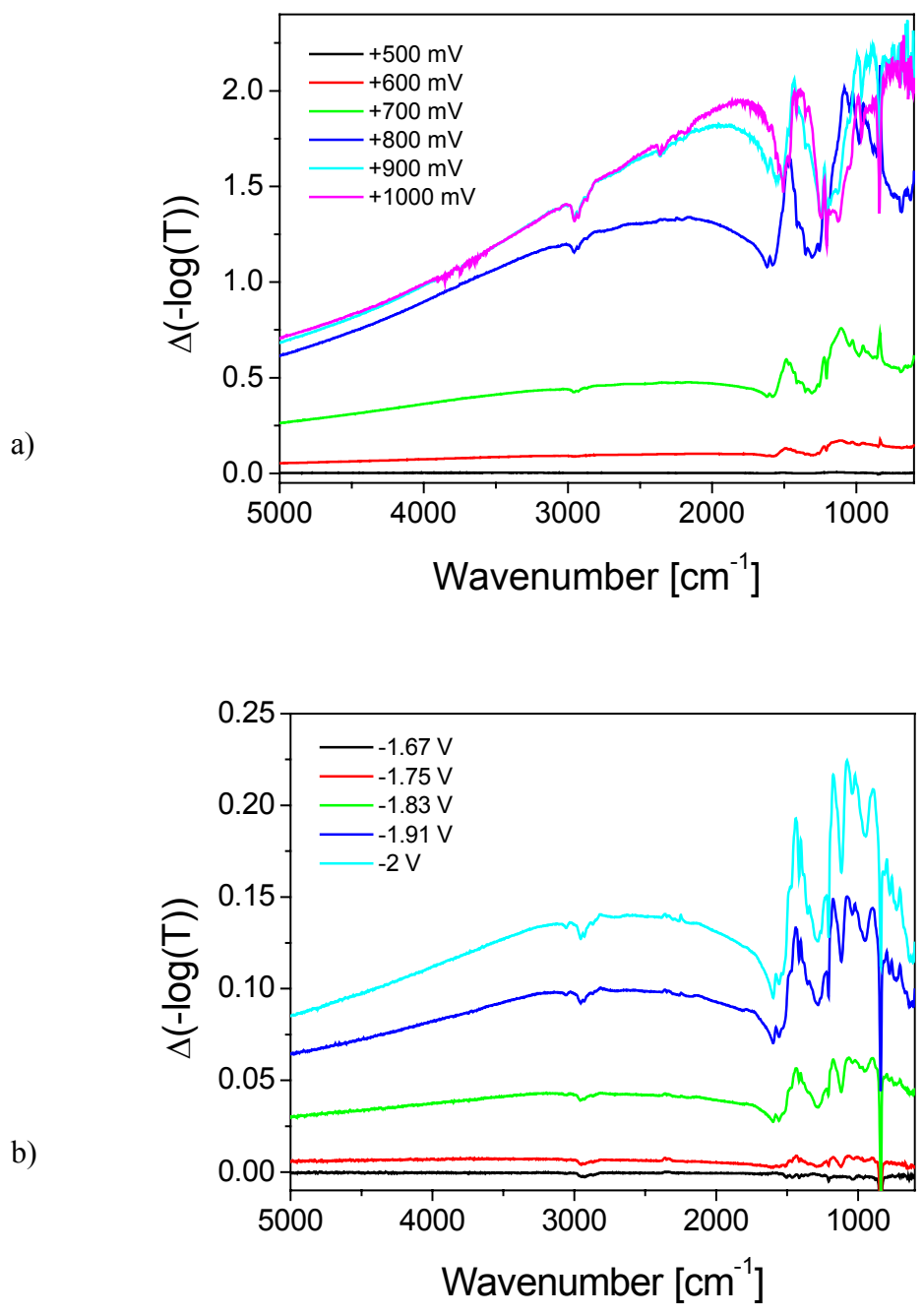


**Fig. 3.7:** Evolution of in situ UV-VIS difference spectra of MDMO-PPV, 10 s in the time scale correspond 100 mV during the CV: a) reduction; b) oxidation

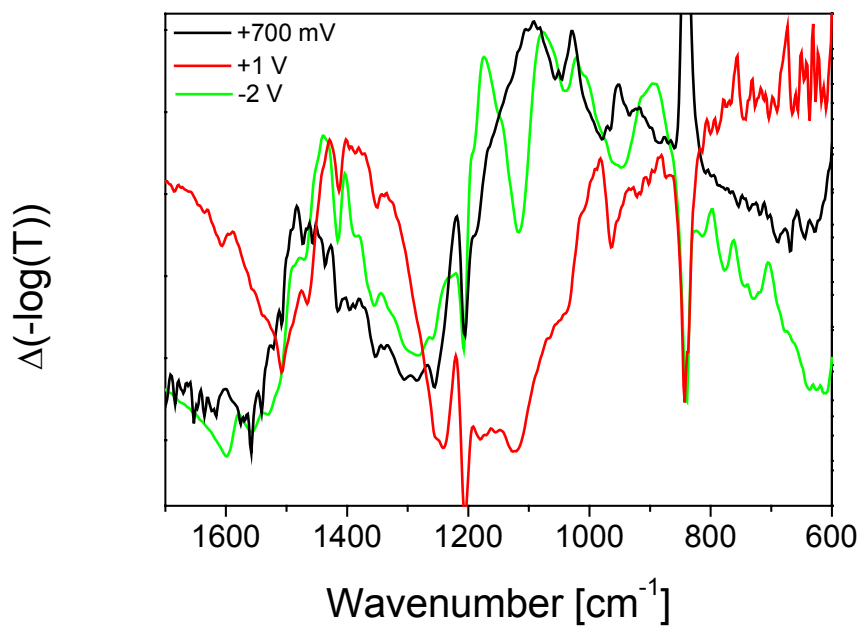
Again the bleaching of the ground state transition can be clearly seen as a negative band in blue color while the evolution of the polaronic band appears in red color as an additional contribution in comparison with the reference spectrum. The optical response of negative charge carriers formed during reduction is not so strong as for the positive charge carriers generated by oxidation. Again it can be seen that both processes are not completely reversible as the reference spectrum of the pristine material is not completely recovered.

Fig. 3.8 shows the in situ FTIR spectra of MDMO-PPV for both p- and n-doping. In the region above  $\sim 1700 \text{ cm}^{-1}$  again a broad band of a polaronic transition can be found. Below  $\sim 1700 \text{ cm}^{-1}$  the so called infrared active vibration (IRAV) modes appear [75-79], which are due to IR activation of the Raman active  $A_g$  modes of the neutral polymer as the symmetry is locally broken around the charge carrier. The strong band around  $830 \text{ cm}^{-1}$  comes from  $\text{PF}_6^-$  which enters and leaves the polymer layer during the electrochemical reactions.

The pattern of the IRAV modes is different from that of unsubstituted PPV [86] but is similar to spectra already found for 2,5-substituted PPV's [87,88]. Fig. 3.9 shows a comparison of the IRAV region for oxidation at lower and higher potentials and reduction. The change of the pattern when going to higher oxidation potentials indicates that another kind of charge carriers is formed there. A clear difference can be seen between oxidation and reduction. Although the broad bands are very similar considering the shape for oxidation at low potentials and reduction, the fine structure looks quite different. Also the intensity of the peaks is not the same for oxidation and reduction [88].



**Fig. 3.8:** In situ FTIR spectra of MDMO-PPV: a) oxidation; b) reduction; all potential values vs. NHE



**Fig. 3.9:** Section of the IRAV modes for oxidation at +700 (black line), +1000 (red line) and -2000 mV (green line)

## 3.2 PTPTB

Poly-(*N*-dodecyl-2,5-bis(2-thienyl)-pyrrole-(2,1,3-benzothiadiazole)), the structure is shown in Fig. 3.10, was designed and synthesized for photovoltaic applications by the group of R.A.J. Janssen at the Eindhoven University of Technology [89]. It is a low-bandgap polymer and was provided to the Johannes Kepler University of Linz for spectroscopic characterization and application testing. The concept to achieve the low-bandgap is the push-pull concept with alternating electron rich *N*-dodecyl-2,5-bis(2-thienyl)pyrrole and electron deficient 2,1,3-benzothiadiazole groups.

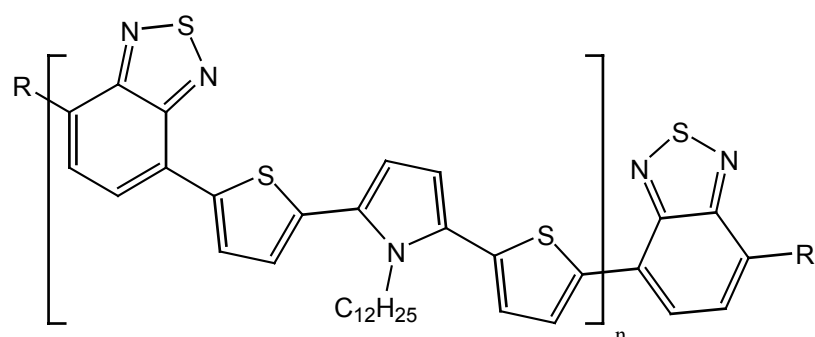


**Fig. 3.10:** Chemical structure of Poly-(*N*-dodecyl-2,5-bis(2-thienyl)-pyrrole-(2,1,3-benzothiadiazole)), PTPTB, R = H, Br, n = 1-4

The usability of this material for polymer solar cells [90-92] and for LED's with near infrared light emission [91,92] has already been shown. However, the exact determination of the band gap and the band edges was of great interest and had to be performed.

### *Electrochemistry*

Fig. 3.11 shows a CV of a PTPTB film dropcast from toluene solution. The approximate onsets around +500 mV for oxidation and -1200mV were the basis for the EVS measurements presented in Fig. 3.12 and Fig. 3.13. As already described for MDMO-PPV the EVS measurements were done several times in different directions on one sample to conclude about the redox stability of the polymer.

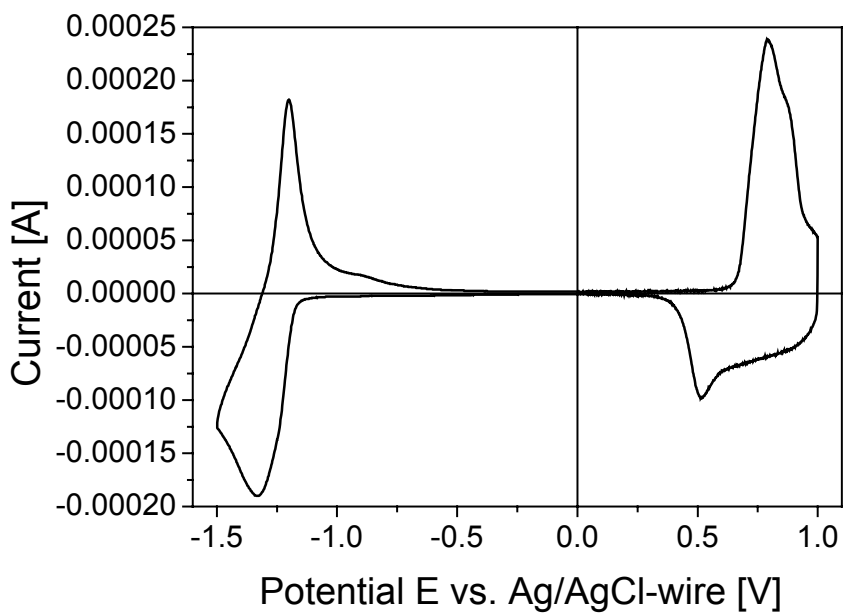


**Fig. 3.11:** Cyclic voltammogram of a PTPTB film, scan rate 10 mV/s,  $E^{1/2}_{\text{Ferrocene}} = 420 \text{ mV}$

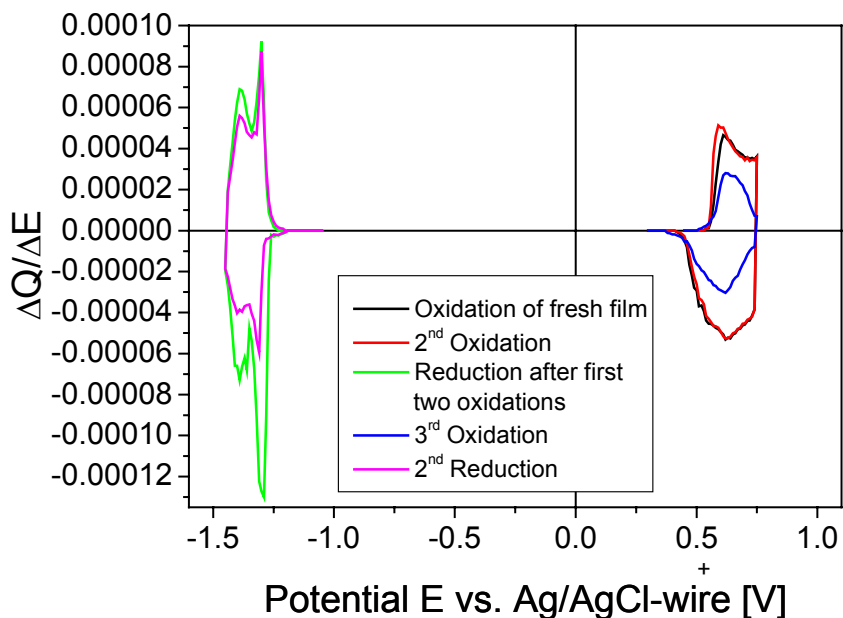


**Fig. 3.12:** EVS measurement for oxidation of PTPTB with subsequent cycles presented in different colours as described in the legend,  $E^{1/2}_{\text{Ferrocene}} = +420 \text{ mV}$ ; the onset determined from the first oxidation was determined at +530 mV vs. NHE

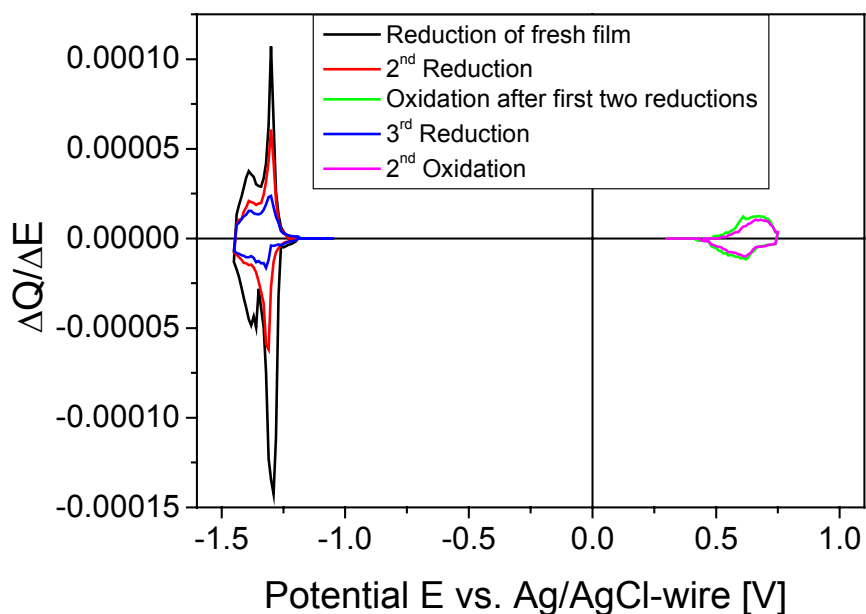


**Fig. 3.13:** EVS measurement for reduction of PTPTB with subsequent cycles presented in different colours as described in the legend,  $E^{1/2}_{\text{Ferrocene}} = +420 \text{ mV}$ ; the onset determined from the first reduction was determined at  $-1230 \text{ mV vs. NHE}$

The onset values for oxidation and reduction were determined from the first measurements on a fresh film at  $+530 \text{ mV}$  and  $-1230 \text{ mV vs. NHE}$ , respectively. This leads to an electrochemical bandgap  $E_g^{\text{EC}}$  of  $1.8 \text{ eV}$ . With value of  $-4.75 \text{ eV vs. vacuum level}$  for the NHE, the band edges for the HOMO and the LUMO can be estimated at  $-5.3 \text{ eV}$  and  $-3.5 \text{ eV}$ .

PTPTB is unstable against cathodic reduction. The changes with subsequent cycling in different potential directions are dramatic if once reduction was performed. The response at positive potentials is different in shape and intensity, but also the reduction peak is decreased. If oxidation is performed as the first process, the reduction wave is observed to be the same as if reduction was the first process. Subsequent reductions lead again to degradation.

A reason for this behaviour could be that there are some bromine atoms as end groups remaining from the precursor substances. These may be reactive centers for further polymerisation reactions or other electrochemical side reactions as, for example, cross linking.

Fig. 3.14 shows the optical absorption of PTPTB at room temperature and after cooling with liquid He and the photoluminescence. As mentioned in the chapter before for this measurement the cryostat was still working and low temperatures could be reached.

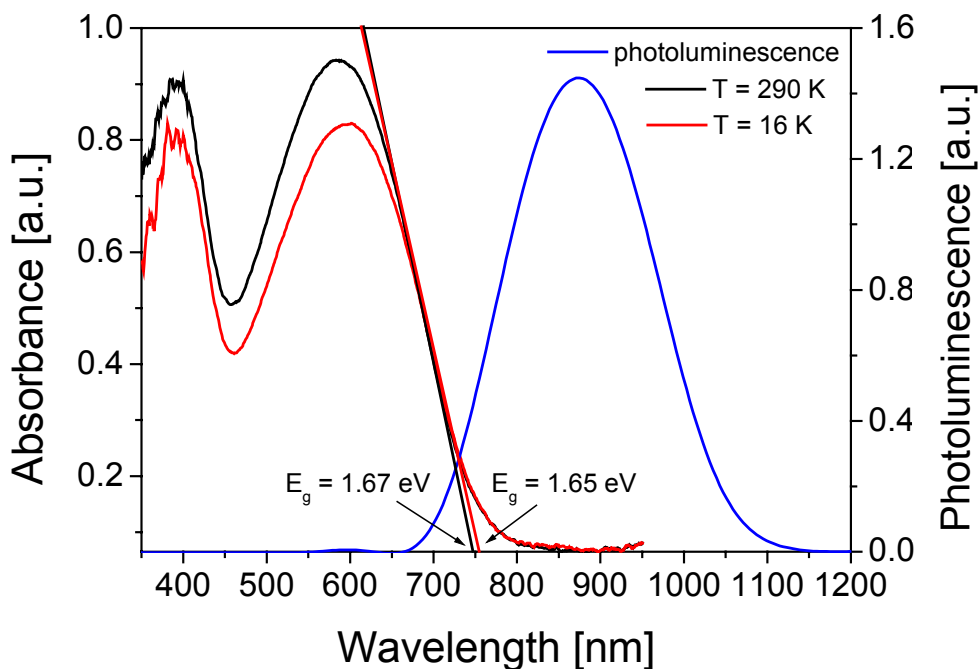


**Fig. 3.14:** Optical absorption and photoluminescence of PTPTB; black line shows the spectrum at room temperature, red line at 16 K, blue line shows the photoluminescence at room temperature (excitation at 488 nm)

As for MDMO-PPV the optical absorption leads to a slightly smaller bandgap as the electrochemically determined value. In this case the spectroscopically found value for  $E_g^{\text{opt}} = 1.7$  eV, which is nevertheless in good agreement with electrochemistry. Photoluminescence occurs as expected [91,92].

Cooling does not affect the value of the band gap dramatically, although a small redshift can be observed for the same reasons as already mentioned in the case of MDMO-PPV. Again also the intensity of the main absorption band decreases. For PTPTB this decrease is more accentuated which can simply be due to the lower temperature achieved for this measurement.

In situ UV-VIS spectroelectrochemistry of PTPTB performed with EVS is depicted in Fig. 3.15. The same experimental parameters were used as for MDMO-PPV.

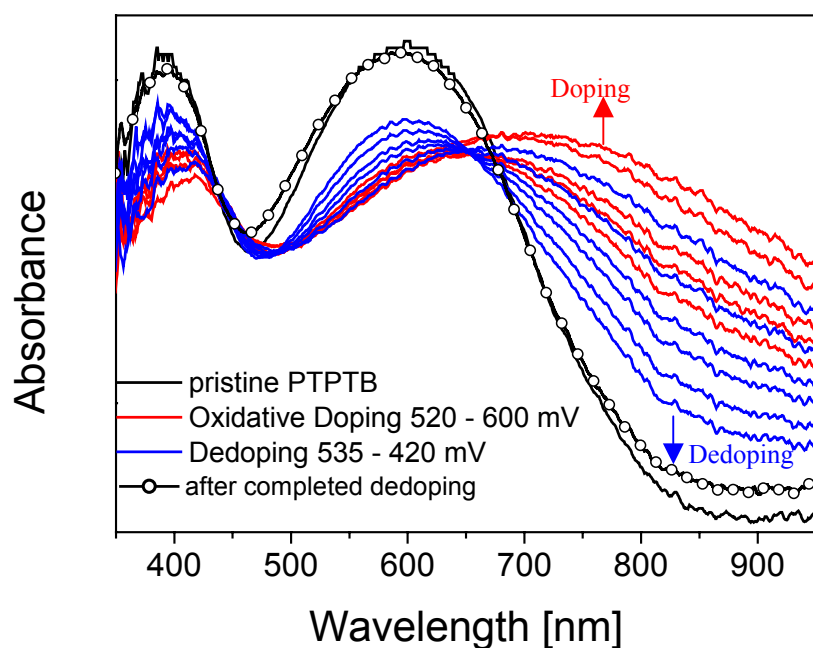


**Fig. 3.15:** In situ UV-VIS spectroelectrochemistry of p- doping of PTPTB: black line pristine polymer; anodic oxidation as red lines from +530 to +850 mV vs. NHE; dedoping as blue lines from +850 to +300 mV vs. NHE, black line with open dots shows the spectrum after dedoping

Only for p-doping clear spectra could be observed for PTPTB. The in situ spectra obtained from p-doping show the typical broad polaron band evolving around 800 nm while the main absorption band is bleached. The oxidation process is nicely reversible as the initial spectrum is almost obtained again. Small differences might be due to both electrochemical side reactions and residual doping.

At least the onset potential for oxidation could be confirmed with this measurement, as for reduction no differences were observed comparing the spectra at different potentials. However, small changes could be found for n-doping doing in situ UV-VIS spectroelectrochemistry with CV. The results from these measurements are shown in Fig. 3.16, again displayed as difference spectra related to the pristine polymer before the measurement.

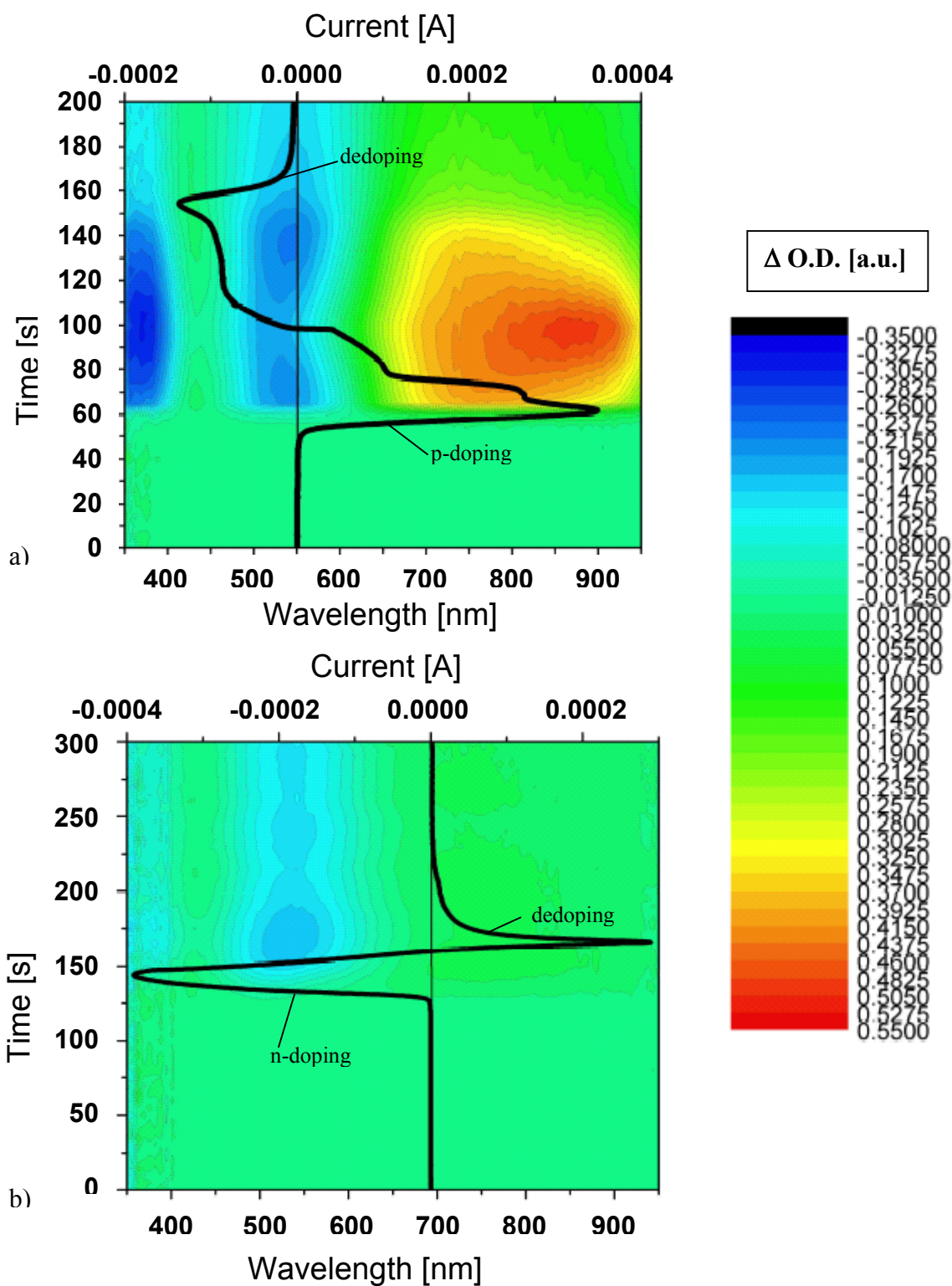


**Fig. 3.16:** Evolution of in situ UV-VIS difference spectra of PTPTB, 10 s in the time scale correspond 100 mV during the CV: a) oxidation; b) reduction

The graph for oxidation clearly shows again the evolution of the polaron band concomitant bleaching of the main absorption band in the ground state. A similar band, but much weaker, could be found for the reduction process of a freshly prepared sample. Although this measurement is not very accurate for onset determination, it can be stated that also the onset for reduction could be confirmed by in situ spectroelectrochemical measurements. The time scale where the cathodic wave starts and where the spectrum of PTPTB changes is the same and corresponds to an onset of  $\sim -1.2$  V.

Also in situ FTIR spectroelectrochemistry has been done on PTPTB. The results are shown in Fig. 3.17 and Fig. 3.18.

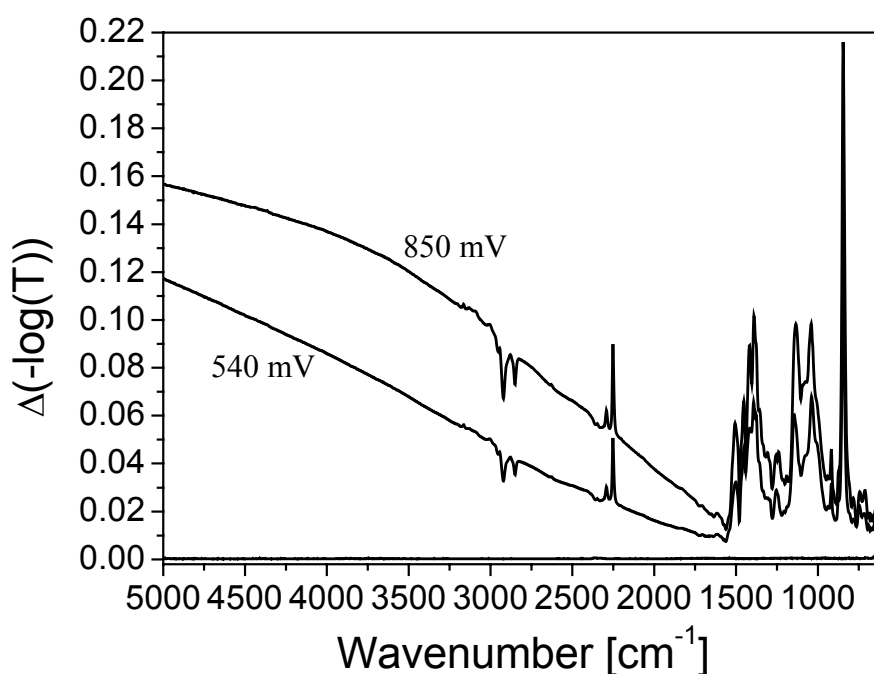


**Fig. 3.17:** In situ FTIR spectra of PTPTB for oxidation; potential between +540 and +850 mV vs. NHE

For the in situ FTIR measurement only for p-doping results could be found. The spectrum shows the typical broad polaron band above  $\sim 1700$   $\text{cm}^{-1}$  and below that value IRAV modes are arising.

Spectral features around  $2300\text{ cm}^{-1}$  and  $2900\text{ cm}^{-1}$  are due to spectral incompensation effects of the electrolyte solution, which cannot be avoided with this technique. Fig. 3.18 shows an enlarged view on the IRAV region. Peaks that are marked with an arrow are due to the electrolyte solution additionally to the peak of  $\text{PF}_6^-$  at  $\sim 830\text{ cm}^{-1}$ . Besides that the bleached bands of the IR spectrum of pristine PTPTB can be found as negative bands superimposed on the IRAV pattern.

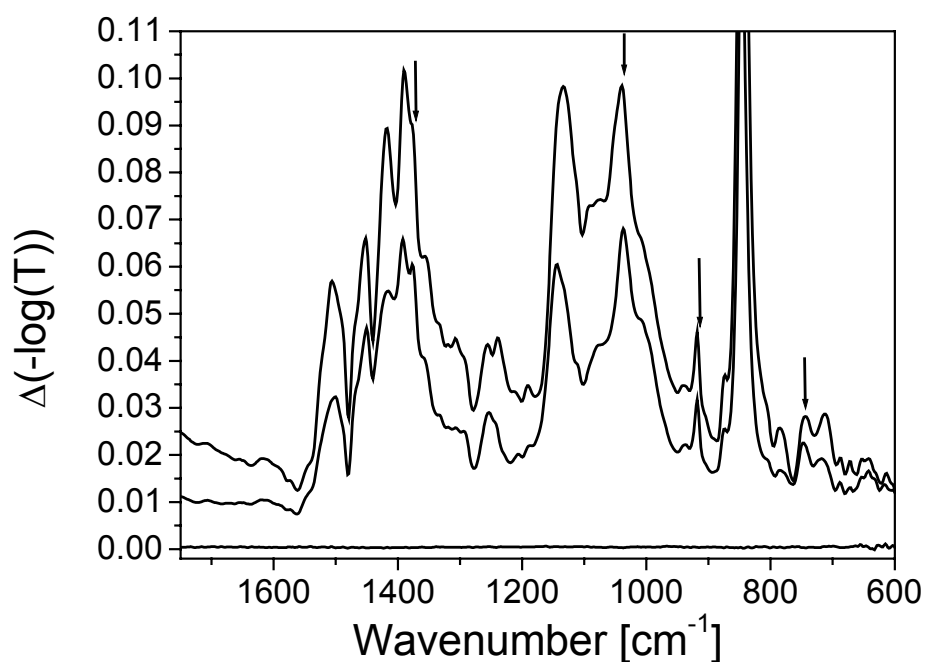


**Fig. 3.18:** Enlarged view on the spectral region of the IRAV modes of electrochemically p-doped PTPTB; the arrows mark bands arising from the electrolyte solution

### 3.3 PEDOT-EHI-ITN

Poly-(3,4-ethylenedioxy-thiophene)-*N*-(2-ethylhexyl)-dicarboxylic-imide-benzo[*c*]thiophene as synthesized at the University of California, Los Angeles, by H. Meng in the group of Prof. F. Wudl [93]. It was provided for spectroscopic characterization and application testing. The structure is shown in Fig. 3.19.

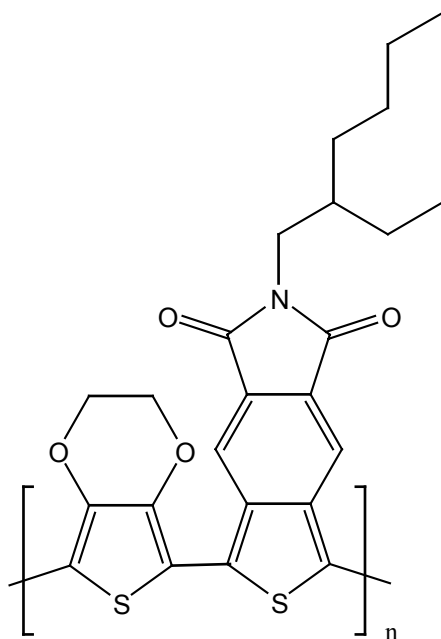


**Fig. 3.19:** Chemical structure of poly-(3,4-ethylenedioxy-thiophene)-*N*-(2-ethylhexyl)-dicarboxylic-imide-benzo[*c*]thiophene

It is a low bandgap polymer with a reported bandgap of 1.1 eV. Polymers with isothionaphthene units polymerized in the backbone have the lowest bandgaps of ~1.0 eV reported for conjugated polymers so far [94]. For this molecule the condensed benzene ring minimizes the bond length alternation along the polymer backbone forcing the interring bonds into a more quinoid character, which leads to the small bandgap [60,95]. Polyisothionaphthene itself however is very unstable at ambient conditions.

The new copolymer, one of a series of different copolymers and polymers, shows improved stability while the band gap is still low.

This material shows an unusually high electron spin resonance signal probably coming from residual doping from the synthesis. A part of the material was dedoped with hydrazine which is known to be a selective reducing agent for conjugated polymers to regain their intrinsic semiconducting properties. In this work both the polymer as it was received and the dedoped material were investigated. No difference in the results could be found for the different samples, therefore no further diversification was done for describing the results.

### *Electrochemistry*

A CV of PEDOT-EHI-ITN is shown in Fig. 3.20. From this CV, using the same method for an estimation of the onset potentials as described in the chapters before, the onset for oxidation should be in the region of  $-300$  mV and for reduction around  $-700$  mV. The CV shows broad and undefined anodic and cathodic waves compared to the other materials.

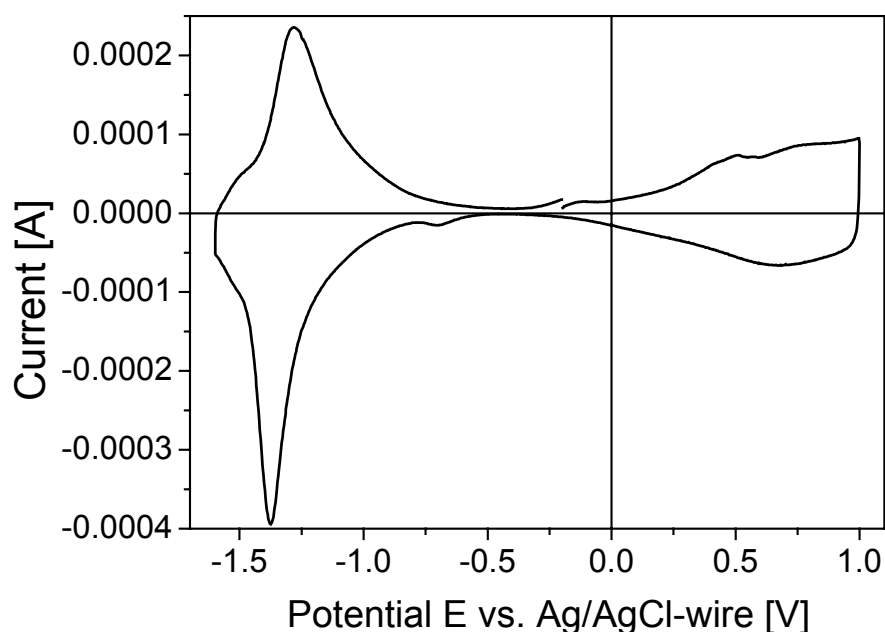


**Fig. 3.20:** Cyclic voltammogram of a PEDOT-EHI-ITN film, scan rate 10 mV/s,  $E_{\text{Ferrocene}}^{1/2} = 420$  mV

For these estimated onset potentials EVS measurements were carried out which are depicted in Fig. 3.21 and Fig. 3.22. As for the other two materials the oxidation and reduction onset potential was determined from a freshly prepared film. For each sample the subsequent cycling was performed.

The onset values for oxidation and reduction were determined at -290 mV and -750 mV vs. NHE, respectively. This leads to an electrochemical bandgap  $E_g^{EC}$  of 0.5 eV. With a value of -4.75 eV vs. vacuum level for the NHE, the band edges for the HOMO and the LUMO can be estimated at -4.5 eV and -4 eV. This result is in strong contradiction to the reported optically determined band gap value of 1.1 eV [86,87]. A check of the EVS results with in situ spectroelectrochemistry should clarify this problem.

The electrochemical behaviour of PEDOT-EHI-ITN concerning stability while cycling is excellent. Neither the onset potential nor the intensity of the anodic or cathodic waves are significantly affected.

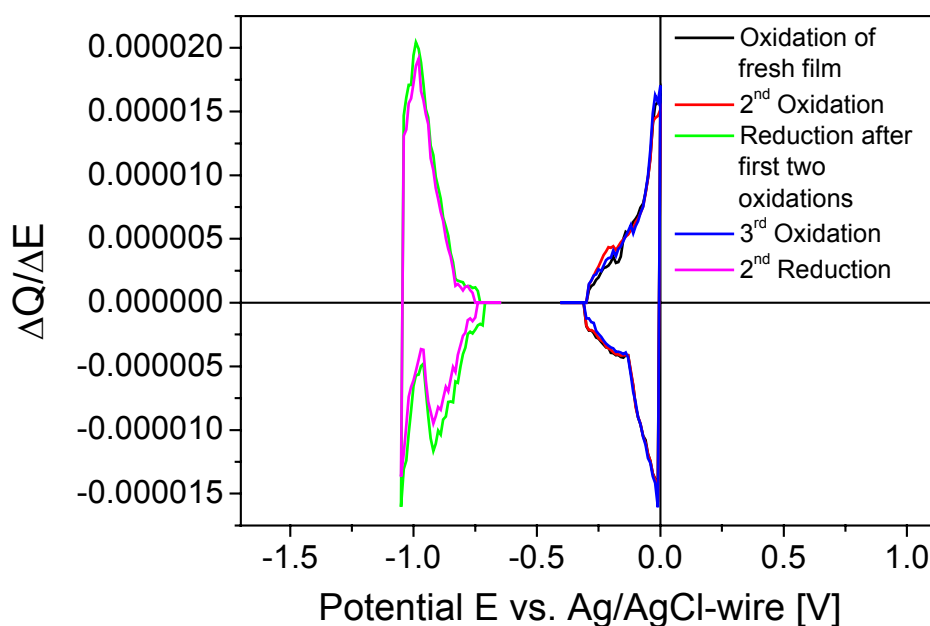


**Fig. 3.21:** EVS measurement for oxidation of PEDOT-EHI-ITN with subsequent cycles presented in different colours as described in the legend,  $E^{1/2}_{\text{Ferrocene}} = +420 \text{ mV}$ ; the onset determined from the first oxidation was determined at -290 mV vs. NHE

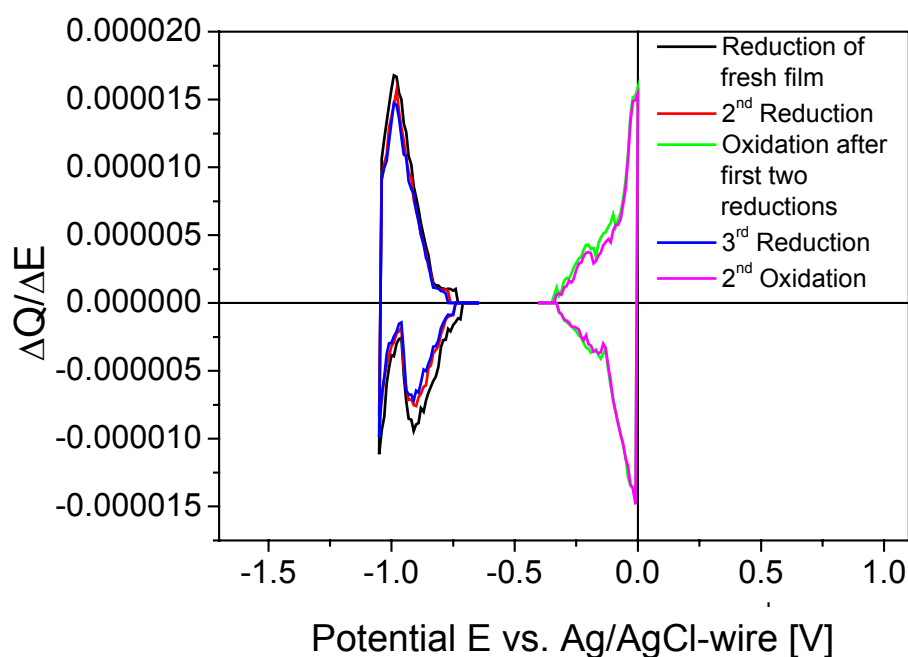


**Fig. 3.22:** EVS measurement for reduction of PEDOT-EHI-ITN with subsequent cycles presented in different colours as described in the legend,  $E_{\text{Ferrocene}}^{1/2} = +420 \text{ mV}$ ; the onset determined from the first reduction was determined at  $-750 \text{ mV vs. NHE}$

Absorption spectroscopy of PEDOT-EHI-ITN was only done in the context with in situ spectroelectrochemistry but the range of the spectrometer used for this purpose was not wide enough to get the optical onset. Other available spectroscopic setups were tested but with none a spectrum useful for the optical determination of the band gap could be obtained as the absorption band of this material is very broad with no sharp edge as for the other materials. At least these measurements showed no evidence for an optical band gap  $E_g^{\text{opt}}$  of  $0.5 \text{ eV}$ . Therefore the value from literature [92,93] of  $1.1 \text{ eV}$  was used for comparison.

### *Spectroelectrochemistry*

In situ UV-VIS spectroelectrochemistry was in this case extremely important to get the electrochemical bandgap. Though polaronic bands could not be seen as the range of spectrometer did not reach for enough to near IR, the bleaching of the main absorption band which was at least to a great portion observable could be observed.

This bleaching gives information on the potential where changes in the electronic system due to doping effects occur. In situ UV-VIS spectra from EVS measurements for oxidation and reduction are shown in Fig. 3.23 and Fig. 3.24, respectively.

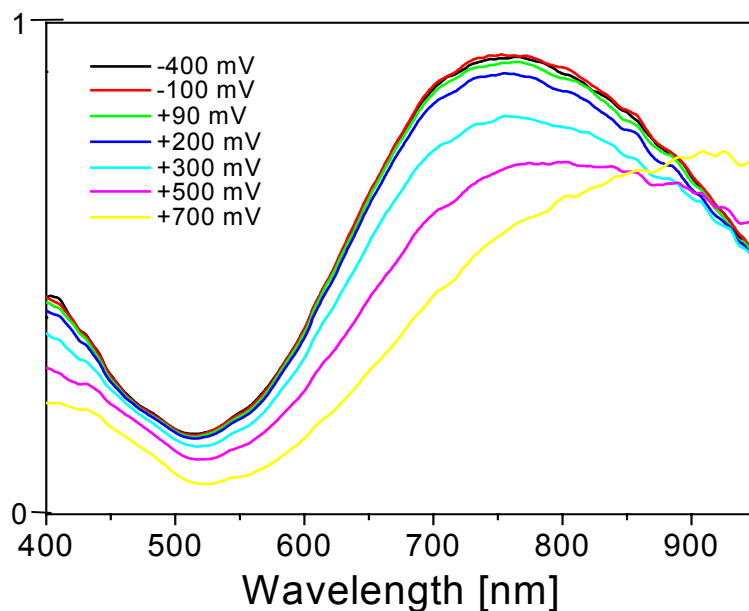


**Fig. 3.23:** In situ UV-VIS spectroelectrochemistry of p- doping of PEDOT-EHI-ITN; all potential values are given vs. NHE; start of bleaching of main absorption band indicates onset potential for oxidation at +90 mV, arbitrarily baseline corrected for gold grid electrode

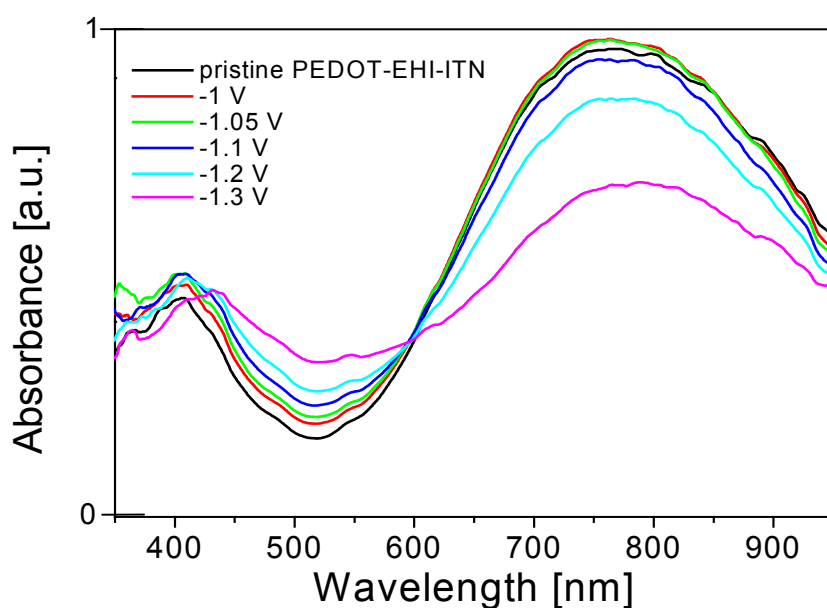


**Fig. 3.24:** In situ UV-VIS spectroelectrochemistry of n- doping of PEDOT-EHI-ITN; all potential values are given vs. NHE; start of bleaching of main absorption band indicates onset potential for reduction at  $-1.1$  V, arbitrarily baseline corrected for gold grid electrode

The start of the bleaching of the main absorption band representing electronic changes in the conjugated polymer backbone indicates onset potentials of +90 mV vs. NHE for oxidation and -1100 mV vs. NHE for reduction. This leads to an electrochemical band gap  $E_g^{EC}$  of 1.2 eV in contrast to 0.5 eV determined solely by EVS. The value is in good agreement with the optical band gap estimation of 1.1 eV. The current flowing at -290 mV vs. NHE in EVS experiments is not accompanied by spectral changes of the conjugated  $\pi$ -electron system.

For oxidation a part of the evolving polaron band concomitant with the bleaching can be seen in Fig. 3.23 around 900 nm. For the reduction measurement the observable spectral range is apparently too small to find such a band as it appears probably further in the IR. Also a clear difference of the spectra obtained during oxidation and reduction can be seen. Especially in the region around 520 nm a very different behaviour can be observed. The intensity of the main absorption band increases in the beginning of reduction, which is an indication of some residual doping from the synthesis as mentioned in the beginning of this chapter.

Again in situ UV-VIS spectroelectrochemistry was also carried out during a CV taking difference spectra related to the pristine polymer. The results are shown in Fig. 3.25.

This measurement gives the same result for the onset determination as the in situ EVS measurements and therefore a misleading smaller value for the band gap can be excluded. The spectral changes do not occur at the onset potentials for both oxidation and reduction found solely with EVS but appear at similar potentials as determined with in situ EVS. In this measurement also the spectral differences of p- and n-doping can be clearly seen again. From the difference spectra also a different shape of the bleaching of the main absorption band can be observed besides the already mentioned different behaviour around 520 nm indicating different ways of charge generation and stabilization for positive and negative charges in this material.

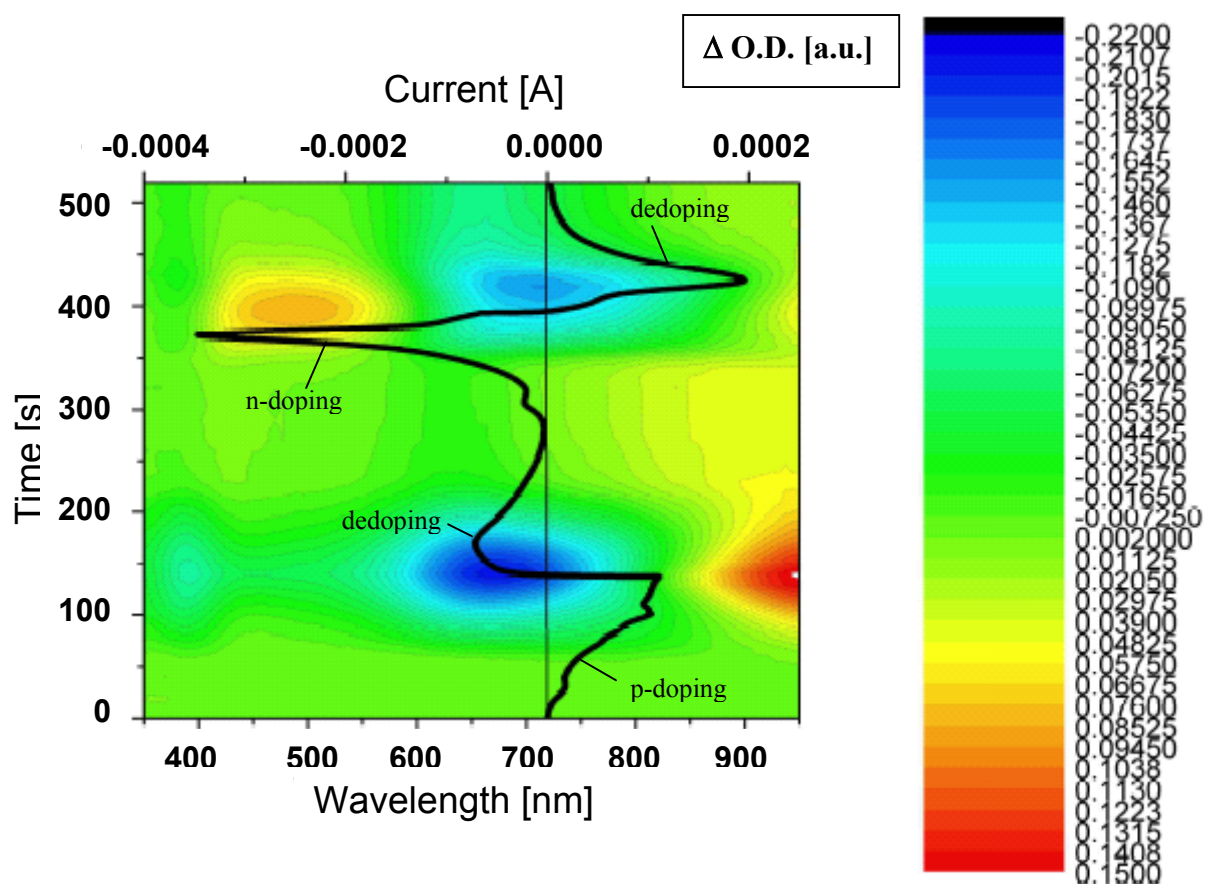


**Fig. 3.25:** Evolution of in situ UV-VIS difference spectra of PEDOT-EHI-ITN for both anodic oxidation and cathodic reduction, 10 s in the time scale correspond 100 mV during the CV

Due to the spectroscopic determination of the doping potentials another EVS was recorded with a wider potential range in both directions. The width of the steps had to be changed to 20 mV as the computer program can only acquire a certain amount of data and would not have been able to collect all data with a step width of 10 mV.

The potential ranges were  $-400$  mV to  $+500$  mV and back for oxidation and  $-650$  mV to  $-1450$  mV and back for reduction. For the second cycle for reduction the lower limit potential was set to  $-510$  mV as the dedoping process was not completely finished at  $-650$  mV. The results are shown in Fig. 3.26.

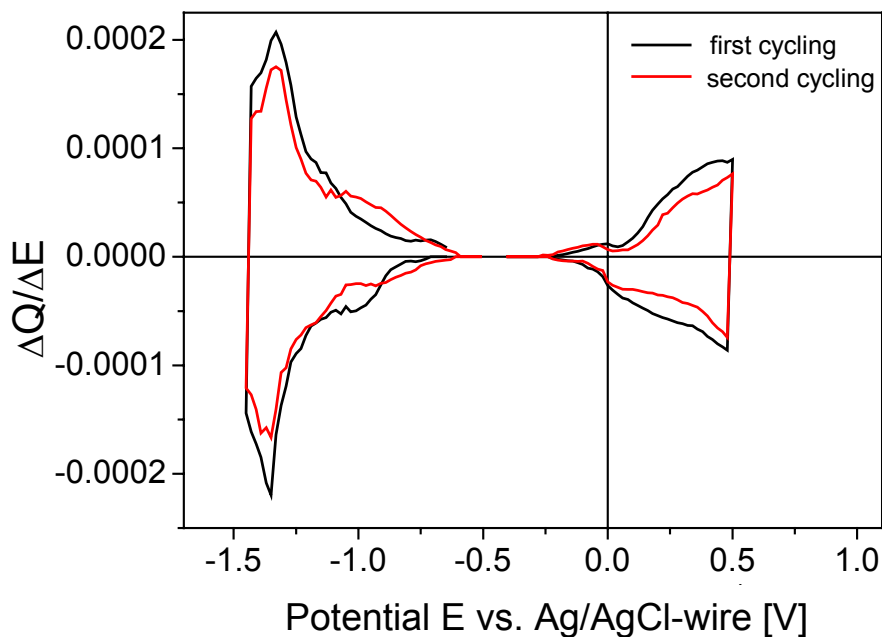


**Fig. 3.26:** EVS measurements on a PEDOT-EHI-ITN film over a wider potential range performed with 20 mV steps;  $E_{\text{Ferrocene}}^{1/2} = 430 \text{ mV}$

Structures in the plot at +100 mV for oxidation and -1100 mV for reduction as additional steps can be seen (similar to structures found in the CV shown in Fig. 3.20), which are related to doping induced changes in the electronic structure of the polymer backbone.

As the waves of the side reactions and the polymer backbone overlap each other a clear determination of the onset potentials is not possible only from EVS measurements. Only from a combination of spectroscopic techniques with electrochemical results a clear determination of the band gap and the band edges for the HOMO and the LUMO is possible

The results show the importance of spectroelectrochemical measurements for characterization of conjugated polymers in the context of band gap and band edge determination. Only when bleaching of the polymer absorption occurs concomitant with an electrochemical reaction the conjugated backbone of the polymer is affected and the desired property can be determined.

### 3.4 PCBM and UCM FG62

For comparison and for determination of the electronic parameters in solar cell mixtures also the electron accepting part, i.e. fullerene derivatives, was characterized with electrochemistry.

1-(3-methoxycarbonyl)-propyl-1-phenyl-(6,6) $C_{61}$  (PCBM) [96] is a soluble fullerene derivative used standardly as the acceptor in bulk heterojunction solar cells. It was provided by Prof J. C. Hummelen (University of Groningen) for scientific investigation on solar cells.

1,1-Bis(4,4'-dodecyloxyphenyl)-(5,6) $C_{61}$  (working designation UCM FG62) was provided by Prof. N. Martin (University of Madrid) for application testing. It is also a fullerene derivative with a different side group that should influence the acceptor behaviour. The chemical structures of the two materials are shown in Fig. 3.27.

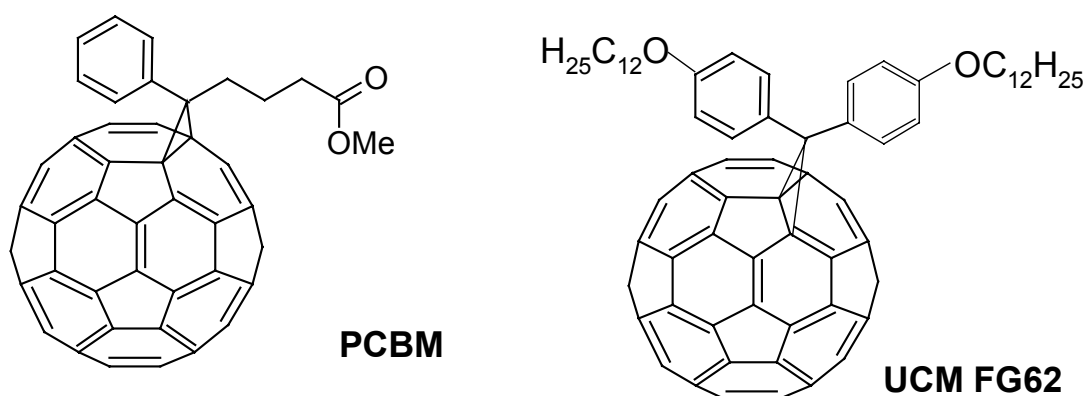


**Fig. 3.27:** Chemical structures of 1-(3-methoxycarbonyl)-propyl-1-phenyl-(6,6) $C_{61}$  (PCBM) and 1,1-bis(4,4'-dodecyloxyphenyl)-(5,6) $C_{61}$  (UCM FG62)

These two materials were electrochemically tested with the use of the microelectrochemical cell. Special interest was put to the first reduction potential of the materials as this characterizes the acceptor strength. From these experiments the LUMO levels of the fullerene derivatives in solution were determined. As a supplement and for comparison the LUMO in solid state was also determined by EVS from a film of each fullerene derivative. As the reduced species of the fullerenes immediately starts dissolving in  $CH_3CN$  no plots of  $\Delta Q/\Delta E$  vs.  $E$  could be obtained. However, the onset potentials for reduction could be determined in this way.

The CV's from solutions measured with the microelectrochemical cell are depicted in Fig. 3.28. As not exactly the same amounts of the materials were dissolved two current axis are used for presentation.

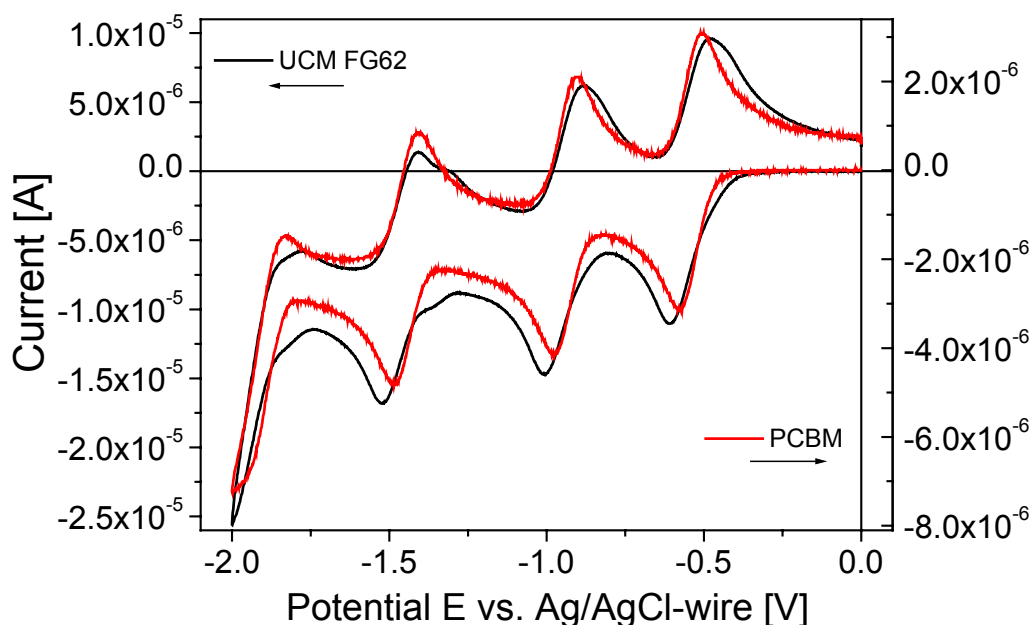


**Fig. 3.28:** CV measurements in solution with a scan rate of 50 mV of PCBM (red line, right scale) and UCM FG62 (black line, left scale); the solvent was a 1 : 4 mixture of  $\text{CH}_3\text{CN}$  and *o*-dichlorobenzene,  $E^{1/2}_{\text{Ferrocene}} = 545$  mV

In the potential range shown three reversible reduction waves typical for fullerenes can be seen. Though the CV's of PCBM and UCM FG62 are slightly different, their first reduction potential and therefore their acceptor strength is the same with a value of  $-690$  mV vs. NHE. This leads to a LUMO level at  $-4.1$  eV vs. vacuum. The value obtained is in good agreement with other already published values for PCBM [96,97], for UCM FG62 no literature values exist so far. Comparing this value with the values found in solid state from EVS shows remarkable differences. For PCBM and UCM FG62 an onset potential of  $-470$  mV vs. NHE was determined leading to a LUMO level of  $-4.3$  eV vs. vacuum.

The question arises, which value better describes the behaviour of the fullerene derivatives as an electron acceptor inside the bulk of a solar cell. Probably the determined onset potential value obtained from EVS in the solid state better reflects this behaviour, but this still has to be proven.

The difference of the LUMO values determined electrochemically from solution and from a solid film should be kept in mind when thinking about the theoretically possible open circuit voltage of organic solar cells. It is defined as the difference between the HOMO level of the polymer as the donor and the LUMO level of the acceptor, in this case the fullerene derivative [97] in contrast to inorganic solar cells where it is determined by the work function difference of the two electrodes. This will be discussed in more detail in the next chapter.

## 4. Summary and Conclusion

### *Summary of the results*

A comparison of the optical band gap  $E_g^{\text{opt}}$  and the electrochemical band gap  $E_g^{\text{EC}}$  is given in Tab. 4.1 for all three polymers. The determined HOMO and LUMO levels are summarized in Fig. 4.1, showing the levels of the substances arranged as in a photovoltaic device.

**Tab. 4.1:** Comparison of the optical band gap  $E_g^{\text{opt}}$  and the electrochemical band gap  $E_g^{\text{EC}}$  for MDMO-PPV, PTPTB and PEDOT-EHI-ITN

	MDMO-PPV	PTPTB	PEDOT-EHI-ITN
$E_g^{\text{opt}}$ [eV]	2.1	1.7	1.1
$E_g^{\text{EC}}$ [eV]	2.3	1.8	1.2 (0.5 solely EVS)

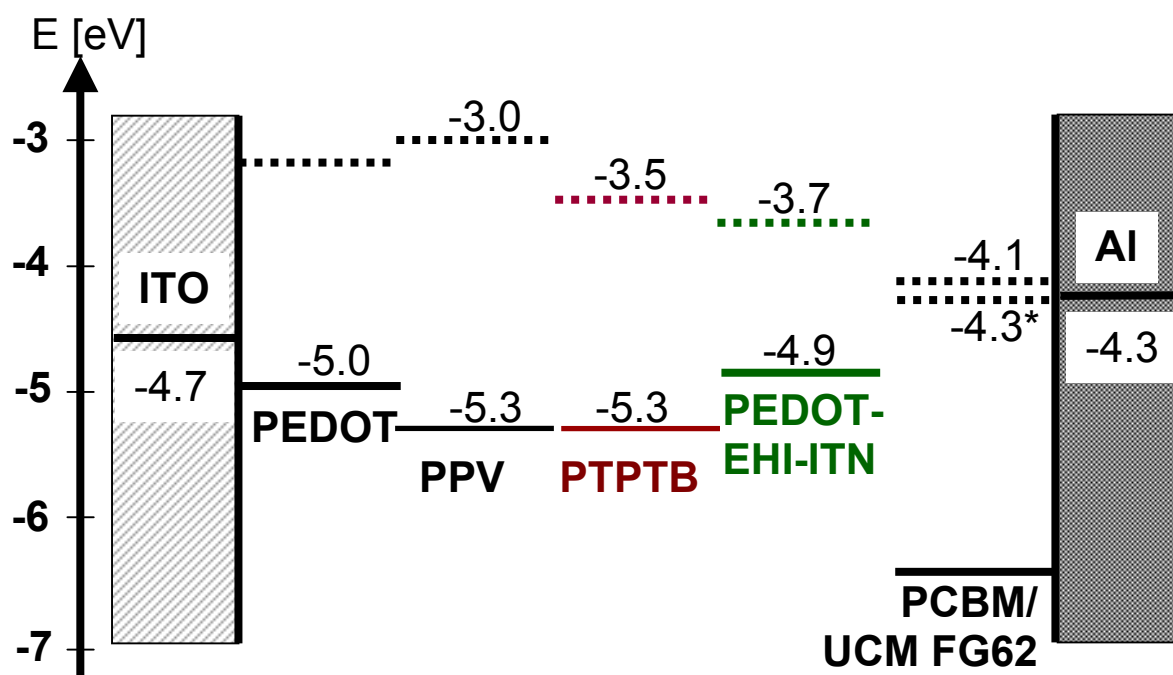


**Fig. 4.1:** Energy diagram for an organic solar cell showing the HOMO and LUMO levels of MDMO-PPV (short as PPV), PTPTB and PEDOT-EHI-ITN calculated from EVS with NHE = 4.75 eV vs. vacuum, \* marks the onset potential for PCBM and UCM FG62 from EVS, the other values origin from the solution CV. The values for ITO (indium tin oxide), PEDOT and Al are taken from literature [98]

Several publications can be found in literature in which the optical and the electrochemical bandgap of conjugated polymer are compared [27,29-31,99-103]. Only in ref. [27,29-31] the electrochemical onset determination was done with EVS although they are already older publications. A clear trend as can be seen from the work presented here with the electrochemical band gap slightly higher than the optical band gap while still in good agreement can be found especially in the works in which EVS was used. A possible explanation for this observation is given in ref. [103]. The optical band gap is considered to be the 'pure' HOMO – LUMO transition while in the electrochemical data generally an interface barrier for charge injection between different materials can play a role. Such a barrier could occur at the interface between the working electrode and the polymer film and therefore increase the observed value. It is also stated that due to this fact and experimental findings the electrochemical system is much closer to the , in this case polymer LED, device design [101,103], which could in turn also be true for polymer solar cells.

For the interpretation of the energy scheme depicted in Fig. 4.1 the above mentioned facts could be helpful. A solar cell consists of indium tin oxide (ITO) covered with a layer of p-doped PEDOT stabilized with poly-(styrenesulfonate) (PSS) as the anode and evaporated Al on top of the active layer as the cathode. The active layer is a mixture of the polymer with a fullerene derivative sandwiched between the electrodes. Light is shone on the device from the ITO side. As can be seen from the scheme all LUMO levels of the polymers are higher in energy than the LUMO levels of the fullerene derivatives PCBM and UCM FG62 and the HOMO levels are below or around the same level of PEDOT. Thus for each polymer an electron that was excited by light from the HOMO to the LUMO can undergo an energetically favourable charge transfer to the acceptor molecules from where the electron can leave the device through the cathode. In the same way it is favourable for the generated positive charge to leave the device through the anode. The principle requirements for photoinduced charge generation and subsequent charge separation are fulfilled for all three polymers, so also the low band gap materials investigated here fit into this energy scheme.

In contrast to conventional inorganic semiconductor systems, where the open circuit voltage  $V_{OC}$  is determined by the difference of the work functions of the electrodes, the  $V_{OC}$  of polymer solar cells is determined by the difference between the HOMO of the polymer and the LUMO of the acceptor, in this case the fullerene [91]. As all polymers have already been tested in photovoltaic devices with PCBM [18,19,89-92,97,104].

Tab. 2 gives an overview on the theoretical values derived from the results presented in this work and obtained values for the  $V_{OC}$  for each polymer.

**Tab. 2:** Comparison of the theoretical and observed open circuit voltage  $V_{OC}^{th}$  and  $V_{OC}^{obs}$  for photovoltaic devices with MDMO-PPV, PTPTB and PEDOT-EHI-ITN mixed with PCBM; the theoretical value is calculated for both values of the electrochemically determined PCBM - LUMO

	MDMO-PPV	PTPTB	PEDOT-EHI-ITN
$V_{OC}^{th}$ (4.3 eV) [mV], solid state	1000	1000	600
$V_{OC}^{th}$ (4.1 eV) [mV], solution	1200	1200	800
$V_{OC}^{obs}$ [mV]	820	720	130

As expected from their HOMO levels the values found for MDMO-PPV and PTPTB devices are quite similar. The reason why the  $V_{OC}$  of PEDOT-EHI-ITN is so low is not clear. Device optimization is necessary for enhancing this  $V_{OC}$  value closer to the theoretical value  $V_{OC}^{th}$ .

Considering the theoretical values for the  $V_{OC}$  in special for MDMO-PPV and PTPTB there is now the question which LUMO value to take for the fullerene acceptors as already indicated in the last chapter. If the mentioned assumption that electrochemistry is a good reference system for polymer LED's and this can be also applied to organic solar cells is true then the  $-4.3$  eV determined from EVS for the fullerene LUMO should be taken. Considering the fullerene LUMO at  $-4.3$  eV the practically obtained  $V_{OC}$  values reach 82% for MDMO-PPV and 72% for PTPTB, which would already be quite good. At lowering the temperature down to 100 K the  $V_{OC}$  of MDMO-PPV/PCBM solar cells increases up to over 900 mV approaching the electrochemical limit [Fig. 9 in 98].

## *Conclusion*

All three newly implemented measurement setups, the microelectrochemical cell, EVS and in situ UV-VIS spectroelectrochemistry, computer controlled with the S.C.A.D.A. software are working and give reliable results. Performing electrochemistry inside a glovebox with an inert atmosphere further enhances the experimental possibilities as the preparation time is significantly decreased and disturbing contributions of water and oxygen can be eliminated.

The determination of HOMO and LUMO levels and concomitant the band gap of conjugated polymers with electrochemical voltage spectroscopy proved to be a very useful method for this purpose. The possibility to confirm these results with in situ spectroelectrochemistry performed during EVS and CV is very important for reliable results. For this purpose specifically in situ UV-VIS spectroelectrochemistry is an appropriate method. The effort necessary for preparation of the experiment for in situ FTIR measurements is higher but shows structural relaxations during doping.

Optically and electrochemically determined values are in good agreement for all three polymers. From the determined HOMO and LUMO levels a rough estimation of the expectable open circuit voltage and a prediction for suitability concerning the energetic possibility for photoinduced charge transfer to a fullerene acceptor in a solar cell can be given.

## 5 References

- [1] H. Shirakawa, E.J. Louis, A.G. MacDiarmid, C.K. Chiang, A.J. Heeger, *J. Chem. Soc. Chem. Comm.*, 1977, 578
- [2] C.K. Chiang, C.R. Fincher Jr, Y.W. Park, A.J. Heeger, H. Shirakawa, E.J. Louis, S.C. Gau, A.G. MacDiarmid, *Phys. Rev. Lett.* **39** (1977), 1098
- [3] C.K. Chiang, M.A. Druy, S.C. Gau, A.J. Heeger, E.J. Louis, A.G. MacDiarmid, Y.W. Park, H. Shirakawa, *J. Am. Chem. Soc.* **100** (1978), 1013
- [4] A.J. Heeger, *J. Phys. Chem. B* **105** (2001), 8475
- [5] D. Meissner, *Photon 2*, 34-37 (1999)
- [6] C.J. Brabec, F. Padinger, N.S. Sariciftci, J.C. Hummelen, *J. Appl. Phys.* **85** (1999), 6866
- [7] M. Granström, K. Petritsch, A.C. Arias, A. Lux, M.R. Andersson, R.H. Friend, *Nature* **395** (1998), 257
- [8] C. Arbizzani, M. Mastragostini, B. Scrosati in *Handbook of Organic Conductive Molecules and Polymers*, Vol. 4, Ed. H.S. Nalwa (John Wiley & Sons, New York, 1997), Chap. 11, 595
- [9] W.A. Gazotti, G. Casalbore-Miceli, A. Geri, M.-A. De Paoli, *Adv. Mater.* **10** (1998), 60
- [10] T.F. Otero in *Handbook of Organic Conductive Molecules and Polymers*, Vol. 4, Ed. H.S. Nalwa (John Wiley & Sons, New York, 1997), Chap. 10, 517
- [11] Y. Yang, A.J. Heeger, *Nature* **372** (1994), 344
- [12] W. Göpel, K.-D. Schierbaum in *Handbook of Organic Conductive Molecules and Polymers*, Vol. 4, Ed. H.S. Nalwa (John Wiley & Sons, New York, 1997), Chap. 12, 621
- [13] J.J.M. Halls, C.A. Walsh, N.C. Greenham, E.A. Marseglia, R.H. Friend, S.C. Moratti, A.B. Holmes, *Nature* **376** (1995), 498
- [14] F. Hide, M. Diaz-Garcia, D. Schwartz, M. Andersson, Q. Pie, A.J. Heeger, *Science* **273** (1996), 1833
- [15] N.S. Sariciftci, A.J. Heeger in *Handbook of Organic Conductive Molecules and Polymers*, Vol. 1, Ed. H.S. Nalwa (John Wiley & Sons, New York, 1997), Chap. 8, 413
- [16] D.O. Reagan, M. Graetzel, *Nature* **353** (1991), 737
- [17] D. Wöhrle, D. Meissner, *Adv. Mat.* **3** (1991), 129

- [18] S.E. Shaheen, C.J. Brabec, N.S. Sariciftci, F. Padinger, T. Fromherz, J.C. Hummelen, *Appl. Phys. Lett.* **78** (2001), 841
- [19] C.J. Brabec, N.S. Sariciftci, J.C. Hummelen, *Adv. Funct. Mater.* **11** (2001), 15
- [20] J.H. Burroughes, D.C.C. Bradley, A.R. Brown, R.N. Marks, K. Mackay, R.H. Friend, P.L. Burns, A.B. Holmes, *Nature* **372** (1990), 539
- [21] D. Braun, *Materialstoday* June 2002, 32
- [22] M. Green, K. Emery, K. Buecher, D.L. King, S. Igari, *Progress in Photovoltaics: Res. Appl.* **5** (1997), 51
- [23] A.H. Thompson, *Phys. Rev. Lett.* **40** (1978), 1511
- [24] A.H. Thompson, *J. Electrochem. Soc.* **126** (1979), 608
- [25] A.H. Thompson, *Rev. Sci. Instrum.* **54** (1983), 229
- [26] J.H. Kaufman, J.W. Kaufer, A.J. Heeger, R. Kaner, A.G. MacDiarmid, *Phys. Rev. B* **26** (1982), 2327
- [27] J.H. Kaufman, T.-C. Chung, A.J. Heeger, *Solid State Commun.* **47** (1983), 585
- [28] T.-C. Chung, J.H. Kaufman, A.J. Heeger, F. Wudl, *Phys. Rev. B* **30** (1984), 702
- [29] J.H. Kaufman, T.-C. Chung, A.J. Heeger, *J. Electrochem. Soc.* **131** (1984), 2847
- [30] H. Eckhardt, L.W. Shacklette, K.Y. Yen, R.L. Elsenbaumer, *J. Chem. Phys.* **91** (1989), 1303
- [31] R.B. Kaner, S.J. Porter, D.P. Nairns, A.G. MacDiarmid, *J. Chem. Phys.* **90** (1989), 5102
- [32] G.P. Evans in *Advances in Electrochemical Science and Engineering*, 2 Volumes, Ed. H. Gerischer and C.W. Tobias (VCH-Wiley, Weinheim, 1990), 1-74
- [33] K. Doblhofer, K. Rajeshwar in *Handbook of Conducting Polymers*, Ed. T.A. Skotheim, R.L. Elsenbaumer, J.R. Reynolds (Marcel Dekker Inc., New York 1998), Chap. 20, 531
- [34] F. Lohmann, *Z. Naturforsch.* **22a** (1967), 843
- [35] *Advances in Electrochemistry and Electrochemical Engineering*, Ed. H. Gerischer, C.W. Tobias (John Wiley, New York, 1977), Vol. 10, 213
- [36] R.J. Gomer, G. Tryson, *J. Chem. Phys.* **66** (1977), 4413
- [37] R. Kötz, H. Neff, K. Müller, *J. Electroanal. Chem.* **215** (1986), 331
- [38] G.M. Barrow, *Physical Chemistry* (WCB/McGraw-Hill Boston, Burr Ridge, Dubuque, Madison, New York, San Francisco, St. Louis, 1996) 6<sup>th</sup> ed., Chap. 10, 11
- [39] J. Heinze in *Topics in Current Chemistry* Vol. 152 (Springer Verlag Berlin Heidelberg, 1990), 1

- [40] M.J. Rice, *Phys. Lett. A* **71** (1979), 152
- [41] W.P. Su, J.R. Schrieffer, A.J. Heeger, *Phys. Rev. Lett.* **42** (1979), 1698
- [42] R. Chance, D.S. Boudreaux, J.L. Bredas, R. Silbey in *Handbook of Conducting Polymers*, Vol. 2, Ed. T.A. Skotheim, (Marcel Dekker Inc., New York 1986), Chap. 24, 825
- [43] J.L. Bredas, R.R. Chance, R.Silbey, *Phys. Rev. B* **26** (1982), 5843
- [44] J.L. Bredas, B. Themans, J.G. Fripiat, J.M. Andre, R.R. Chance, *Phys. Rev. B* **29** (1984), 6761
- [45] J.L. Bredas, G.B. Street, *Acc. Chem. Res.* **18** (1985), 309
- [46] H. Kuzmany, M. Mehring, S. Roth (eds.), *Electronic Properties of Conjugated Polymers*, Vol. III, *Basic Models and Applications* (Springer Verlag Berlin Heidelberg, 1989)
- [47] J. Roncali, *Chem. Rev.* **92** (1992), 711
- [48] P. Damlin, C. Kvarnström, A. Ivaska, *Electrochim. Acta* **44** (1999), 4087
- [49] A.F. Diaz, J. Bargon in *Handbook of Conducting Polymers*, Vol. 1, Ed. T.A. Skotheim, (Marcel Dekker Inc., New York 1986), Chap. 3, 81
- [50] G. Zotti in *Handbook of Organic Conductive Molecules and Polymers*, Vol. 2, Ed. H.S. Nalwa (John Wiley & Sons, New York, 1997), Chap. 4, 137
- [51] P.J. Nigrey, A.G. MacDiarmid, A.J. Heeger, *J. Chem. Soc. Chem. Comm.* **96** (1979), 594
- [52] J.L. Bredas in *Handbook of Conducting Polymers*, Vol. 2, Ed. T.A. Skotheim, (Marcel Dekker Inc., New York 1986), Chap. 25, 859
- [53] J. Tanaka, M. Tanaka in *Handbook of Conducting Polymers*, Vol. 2, Ed. T.A. Skotheim, (Marcel Dekker Inc., New York 1986), Chap. 35, 1269
- [54] M. Zagorska, A. Pron, S. Lefrant in *Handbook of Organic Conductive Molecules and Polymers*, Vol. 3, Ed. H.S. Nalwa (John Wiley & Sons, New York, 1997), Chap. 4, 183
- [55] R.E. Peierls, *Quantum theory of solids* (Oxford University Press, London, 1955)
- [56] M. Kertesz, J. Koller, A. Azman, *J. Chem. Phys.* **67** (1977), 1189
- [57] J.P. Lowe, S.A. Kafafi, *J. Am. Chem. Soc.* **106** (1984), 5837
- [58] J.L. Bredas, *J. Chem. Phys.* **82** (1985), 1189
- [59] Y.-S. Lee, M. Kertesz, *J. Chem. Phys.* **88** (1988), 2609
- [60] J. Roncali, *Chem. Rev.* **97** (1997), 173

- [61] Kieboms, R. Menon in *Handbook of Advanced Electronic and Photonic Materials and Devices*, Vol. 8, Ed. H.S. Nalwa, (John Wiley & Sons, New York, 2000), Chap. 1, 1, esp. 33-47
- [62] J.L. Bredas, D. Beljonne, Z. Shuai, J.M. Toussaint, *Synth. Met.* **41-43** (1991), 3743
- [63] E.L. Frankevich, A.A. Lymrev, I. Sokolik, F.E. Karasz, S. Blumstengl, R.H. Baughman, H.H. Horhold, *Phys. Rev. B* **46** (1992), 9320
- [64] E. Conwell in *Primary Photoexcitations in Conjugated Polymers: Molecular Exciton versus Semiconductor Band Model*, Ed. N.S. Sariciftci (World Scientific Publishing, Singapore, New Jersey, London, Hong Kong, 1997), Chap. 16, 489,
- [65] H. Angerstein-Kozłowska, J. Klinger, B.E. Conway, *J. Electroanal. Chem.* **75** (1977), 45, 61
- [66] R.F. Lane, A.T. Hubbard, *J. Phys. Chem.* **77** (1978), 1401
- [67] E. Laviron, *J. Electroanal. Chem.* **100** (1979), 263
- [68] A.T. Hubbard, *J. Electroanal. Chem.* **22** (1974), 165
- [69] E. Laviron, *J. Electroanal. Chem.* **52** (1974), 355, 395
- [70] H. Angerstein-Kozłowska, B.E. Conway, J. Klinger, *J. Electroanal. Chem.* **87** (1978), 301, 321
- [71] J.L. Bredas, R. Silbey, D.S. Boudreaux, R.R. Chance, *J. Am. Chem. Soc.* **105** (1983), 6555
- [72] R.A. Bull, F.F. Fan, A.J. Bard, *J. Electrochem. Soc.* **129** (1982), 1009
- [73] S.W. Feldberg, *J. Am. Chem. Soc.* **106** (1984), 4671
- [74] M. Eiermann, R.G. Hicks, B.W. Knight, F. Wudl, to be published
- [75] B. Horovitz, *Solid State Commun.* **41** (1982), 729
- [76] E. Ehrenfreund, Z.V. Vardeny, O. Brafman, B. Horovitz, *Phys. Rev. B* **36** (1987), 1535
- [77] M. Del Zoppo, C. Castiglioni, P. Zuliani, G. Zerbi in *Handbook of Conducting Polymers*, Ed. T.A. Skotheim, R.L. Elsenbaumer, J.R. Reynolds, (Marcel Dekker, New York, 1998), Chap. 28, 765
- [78] A. Girlando, A. Painelli, Z.G. Soos, *J. Chem. Phys.* **98** (1993), 7459
- [79] E. Ehrenfreund, Z.V. Vardeny, *Proc. SPIE* **3145** (1997), 324
- [80] H. Neugebauer, N.S. Sariciftci in *Lower Dimensional Systems and Molecular Electronics*, Nato ASI series, Series B: Physics, Vol. 248, Ed. R.M. Metzger, P. Day, G.C. Papavassiliou, (Plenum Press, New York, 1991), 401
- [81] H. Neugebauer, *Macromol. Symp.* **94** (1995), 61

- [82] C. Kvarnström, H. Neugebauer, A. Ivaska in *Advanced Functional Molecules and Polymers*, Vol.2, Ed. H.S. Nalwa, (Gordon & Breach: Langhorne, PA, 2001), Chap. 3
- [83] M.W. Urban, *Attenuated Total Reflection Spectroscopy of Polymers*, Am. Chem. Soc., Washington D.C., 1996
- [84] for example L.F. Santos, L.M. Carvalho, F.E.G. Guimaraes, D. Goncalves, R.M. Fabia, *Synth. Met.* **121** (2001), 1697
- [85] for example J. Liu, Y. Shi, Y. Yang, *Appl. Phys. Lett.* **79** (2001), 578
- [86] H. Neugebauer, S. Srinivasan, S. Tasch, G. Leising, N.S. Sariciftci, *Proceedings of the SPIE* **3145** (1997), 507
- [87] S. Srinivasan, H. Neugebauer, N.S. Sariciftci, *Synth. Met.* **84** (1997), 635
- [88] P.B. Miranda, D. Moses, A.J. Heeger, *Phys. Rev. B* **64** (2001), 081201-1
- [89] A. Dhanabalan, P.A. van Hal, J.K.J. van Duren, J.L.J. van Dongen, R.A.J. Janssen, *Synth. Met.* **119** (2001), 169
- [90] A. Dhanabalan, J.K.J. van Duren, P.A. van Hal, J.L.J. van Dongen, R.A.J. Janssen, *Adv. Funct. Mat.* **11** (2001), 255
- [91] C. Winder, G. Matt, J.C. Hummelen, R.A.J. Janssen, N.S. Sariciftci, C.J. Brabec, *Thin Solid Films* **403-404** (2002), 373
- [92] C. Winder, diploma thesis on *Sensitization of Low Bandgap Polymer Bulk Heterojunction Solar Cells*
- [93] H. Meng, F. Wudl, to be published
- [94] F. Wudl, M. Kobayashi, A.J. Heeger, *J. Org. Chem.* **49** (1984), 3382
- [95] J.L. Bredas, A.J. Heeger, F. Wudl, *J. Chem. Phys.* **85** (1985), 4673
- [96] J.C. Hummelen, B.W. Knight, F. Lepec, F. Wudl, J. Yao, C.L. Wilkins, *J. Org. Chem.* **60** (1995), 532
- [97] C.J. Brabec, A. Cravino, D. Meissner, N.S. Sariciftci, T. Fromherz, M.T. Rispens, L. Sanchez, J.C. Hummelen, *Adv. Funct. Mat.* **11** (2001), 374
- [98] V. Dyakonov, *Phys. E*, in press
- [99] C. Arbizzani, M. Catellani, M. Mastragostino, M.G. Cerroni, *J. Electroanal. Chem.* **423** (1997), 23
- [100] U. Schlick, F. Teichert, M. Hanack, *Synth. Met.* **92** (1998), 75
- [101] S. Janietz, D.D.C. Bradley, M. Grell, C. Giebeler, M. Inbasekran, E.P. Woo, *Appl. Phys. Lett.* **73** (1998), 2453
- [102] M. Catellani, R. Lazzatoni, S. Luzzati, J.L. Bredas, *Synth. Met.* **101** (1999), 175

- [103] M. Cheng, Y. Xiao, W.-L. Yu, Z.-K. Chen, Y.-H. Lai, W. Huang, *Thin Solid Films* **363** (2000), 110
- [104] A. Cravino, M. A. Loi, M. C. Scharber, C. Winder, H. Neugebauer, P. Denk, H. Meng, Y. Chen, F. Wudl, N. S. Sariciftci, submitted to *Synth. Met.*

# Curriculum Vitae

Linz, September 2002

## Angaben zu meiner Person

- Geboren am 04.03.1976 in Salzburg
- Familienstand: ledig

## Schulbildung

- 1982-1986 VS Seekirchen am Wallersee
- 1986-1994 Akademisches Gymnasium BG1 Salzburg
- 1995-2002 Studium an der Johannes Kepler Universität Linz: Wirtsch.ing.wesen  
Technische Chemie (WITECH)

## Präsenzdienst

- 1994-1995 ABC-Abwehr/Schwarzenbergkaserne, Salzburg

## Sprachkenntnisse

- Englisch: fließend und verhandlungssicher

## Interessen

- Wissenschaftlich: Photovoltaik, konjugierte Polymere
- Privat: Sport, Musik

## Bisherige Arbeitgeber:

- Sommer 1993: ADEG Zentrale Bergheim
- Sommer 1994-1995: Raiffeisenverband Salzburg

# Curriculum Vitae

Linz, September 2002

## Personal data

- Born on the 4<sup>th</sup> of March 1976 in Salzburg, Austria
- Martial status: unwed

## Education

- 1982-1986 primary school Seekirchen am Wallersee
- 1986-1994 Grammar school BG1 in Salzburg
- 1995-2002 studies at the Johannes Kepler University of Linz: technical chemistry and management

## Military service

- 1994-1995 NBC defense/Schwarzenbergkaserne, Salzburg

## Foreign languages

- English: business fluent

## Interests

- Scientific: photovoltaics, conjugated polymers
- Private: sports, music

## Employers

- Summer 1993: ADEG central Bergheim
- Summer 1994-1995: Raiffeisenverband Salzburg

## List of Publications

- Sensitization of Photoconductive Polyimides for Photovoltaic Applications  
D. Mühlbacher, C.J. Brabec, N.S. Sariciftci, B.V. Kotov, V.I. Berendyaev, B.M. Rumyantsev, J.C. Hummelen  
*Synth. Met.* **121** (2001), 1609
- Comparison of Electrochemical and Spectroscopic Data of the Low Bandgap Polymer PTPTB  
D. Mühlbacher, H. Neugebauer, A. Cravino, N.S. Sariciftci, J.K.J. van Duren, A. Dhanabalan, P.A. van Hal, R.A.J. Janssen, J.C. Hummelen  
Submitted to *Molecular Crystals*
- Polymer Solar Cells and Infrared Light Emitting Diodes: Dual Function Low Bandgap Polymer  
C. Winder, D. Mühlbacher, H. Neugebauer, N.S. Sariciftci, C.J. Brabec, R.A.J. Janssen, J.C. Hummelen  
Submitted to *Molecular Crystals*
- Comparison of the electrochemical and optical bandgap of low-bandgap polymers  
D. Mühlbacher, A. Cravino, H. Neugebauer, N.S. Sariciftci  
Submitted to *Synthetic Metals*

## Contribution to Conferences

- Sensitization of Photoconductive Polyimides for Photovoltaic Applications, D. Mühlbacher, C.J. Brabec, N.S. Sariciftci, B.V. Kotov, V.I. Berendyaev, B.M. Rumyantsev, J.C. Hummelen, ICSM 2000 Gastein
- Comparison of Electrochemical and Spectroscopic Data of the Low Bandgap Polymer PTPTB, D. Mühlbacher, H. Neugebauer, A. Cravino, N.S. Sariciftci, J.K.J. van Duren, A. Dhanabalan, P.A. van Hal, R.A.J. Janssen, J.C. Hummelen, ICEPOM-4 Lviv